nature neuroscience

ARTICLES

https://doi.org/10.1038/s41593-021-00828-2

An amygdala-to-hypothalamus circuit for social reward

Rongfeng K. Hu[1,2], Yanning Zuo[1,2], Truong Ly[1,2], Jun Wang[1,2], Pratap Meera[2], Ye Emily Wu[1,2] and Weizhe Hong[1,2] ✉

Social interactions and relationships are often rewarding, but the neural mechanisms through which social interaction drives positive experience remain poorly understood. In this study, we developed an automated operant conditioning system to measure social reward in mice and found that adult mice of both sexes display robust reinforcement of social interaction. Through cell-type-specific manipulations, we identified a crucial role for GABAergic neurons in the medial amygdala (MeA) in promoting the positive reinforcement of social interaction. Moreover, MeA GABAergic neurons mediate social reinforcement behavior through their projections to the medial preoptic area (MPOA) and promote dopamine release in the nucleus accumbens. Finally, activation of this MeA-to-MPOA circuit can robustly overcome avoidance behavior. Together, these findings establish the MeA as a key node for regulating social reward in both sexes, providing new insights into the regulation of social reward beyond the classic mesolimbic reward system.

Sociality is essential for survival and health in many animal species, including humans, and provides considerable adaptive benefits[1,2]. To fruitfully navigate a social environment, animals must process social and non-social information within immediate and long-term social contexts to make appropriate social decisions[3]. One key piece of information that motivates such decisions is social reward—a rewarding experience associated with social interaction that provides positive reinforcement[4]. Characteristic abnormalities in reward processing, such as those seen in autism spectrum disorders, depression and schizophrenia[5–7], likely represent inappropriate integration of such information. However, how social interaction is reinforcing and leads to a positive experience remains poorly understood.

Previous studies showed that social reward processing involves the classic mesolimbic reward system, including the nucleus accumbens (NAc) and ventral tegmental area (VTA) as well as the brain areas that directly connect to them[8–11]. These are the same brain areas that also process non-social reward signals[5,9,10]. As social reward requires recognition and processing of social cues, the regulation of social reward might also engage circuits beyond the classical reward system, such as those that are specifically involved in social behavior. Although brain areas have been found to directly control specific types of social decisions in a context-dependent manner (for example, aggression, mating and parenting), how these social circuits contribute to social reward remains poorly understood[12–15]. Importantly, a brain area that is implicated in processing social cues and regulating acute behaviors is not necessarily involved in driving the positive reinforcement of social interaction[16–18]. For example, although the ventromedial hypothalamus has been shown to regulate aggression and aggressive motivation, it does not appear to promote positive reinforcement[16]. This suggests that social reward signaling requires engagement with specific neural circuits and cell populations even within social brain areas.

In mice, the MeA is one of the main brain areas mediating social behaviors downstream of olfactory and pheromonal processing[19–22]. Previous work has suggested an important role for the MeA in regulating specific types of social behaviors, including aggressive behavior in males, mating responses in females and parental care toward offspring[12,13,23–26]. Because these specific, moment-by-moment behavioral actions are regulated in a manner that is highly dependent on sex and behavioral context, it remains unclear whether the MeA is involved in positive reinforcement of general social interaction. In this study, we developed an automated operant conditioning paradigm based on previous work to measure general social reward in mice[16,27–29]. We found that adult animals, both male and female, display robust reinforcement of social interaction independent of aggressive or mating contexts. Through cell-type-specific manipulations, we found that activation of the MPOA-projecting MeA circuit is both necessary and sufficient for this positive reinforcement. Interestingly, activating MeA neurons triggers the release of dopamine in the NAc, suggesting that the MeA is a critical circuit component that mediates social reward upstream of the classical reward system.

Results

Adult animals display robust social reward behavior. To effectively measure social reward in adult animals, we developed an operant conditioning task in which subjects nose-poke to gain access to and interact with a target animal (Fig. 1a), based on previous work[16,27–29]. Here, a closed-loop, fully automated system was designed to avoid any perturbations from experimenters during the assay (Fig. 1a). Juvenile animals were used as target animals to probe the response to general social interaction without the involvement of aggression or mating behavior[30,31]. Indeed, both male and female adult animals predominantly displayed close social investigation toward juvenile animals with little aggression or mating during free social interactions (Extended Data Fig. 1a–c).

During this experiment, a subject animal can freely nose-poke two ports. Poking the social port automatically opens a gate 3 s after poking, allowing the subject to closely interact with the target animal for 7 s (Methods and Fig. 1b,c), whereas poking the null port leads to a 10-s timeout. To account for individual bias toward

[1]Department of Biological Chemistry, David Geffen School of Medicine, University of California, Los Angeles, Los Angeles, CA, USA. [2]Department of Neurobiology, David Geffen School of Medicine, University of California, Los Angeles, Los Angeles, CA, USA. ✉e-mail: whong@ucla.edu

a specific port that is unrelated to social preference, we first measured the subject animal's baseline preference for the two ports without presentation of a target animal. Each mouse's less-favored port was designated as the social port for this particular animal in subsequent experiments. Within 7 d, most mice developed a strong preference for and increased poking rate toward the social port (Fig. 1c–e,i,j and Extended Data Fig. 1d,h) but did not display this preference when they were trained without presentation of a target animal (gate opening only, Fig. 1f–h,k,l and Extended Data Fig. 1e). Notably, more than 90% of the pokes in the social port were followed by social interactions, suggesting that poking the social port indeed reflects a motivation to engage in social interaction, rather than a motivation to induce gate opening (Extended Data Fig. 1f). Overall, 70% of the animals showed a consistent preference for the social port after training (Extended Data Fig. 1g). We also examined the performance of both male and female adult mice and found that both males and females developed a strong preference for the social port (Extended Data Fig. 2). This suggests that social interactions are intrinsically rewarding in both males and females and can drive positive reinforcement in an operant conditioning paradigm.

Interestingly, over the course of training, animals not only increased the numbers of pokes in the social port but also exhibited anticipatory behavior that was characterized by waiting in front of the gate during the delay period before opening of the gate and subsequent social interaction. The frequency and duration of this behavior increased after 7 d of training and were significantly higher with the social port than the null port (Fig. 1m,n). Over the course of training, animals also spent increased time engaged in social interaction and displayed reduced latency to initiate social interaction (Fig. 1o,p; as the gate does not open when poking the null port, a social interaction epoch is defined as standing in front of the gate attempting to interact with animals behind the closed gate). These behavioral features demonstrate that adult mice of both sexes display robust social reward behavior.

MeApd Vgat$^+$ neurons are required for social reward. The posterodorsal subdivision of medial amygdala (MeApd) has been implicated in controlling acute social behavioral decisions, such as aggression and parenting behavior[12,13,24]. However, the MeApd has not been associated with positive reinforcement of social behavior. We first asked whether the MeApd is required for social reward behavior. To this end, we performed cell-type-specific ablation of MeApd Vgat$^+$ neurons by expressing Cre-dependent caspase-3 (or EYFP as a control) in the MeApd of Vgat-Cre animals (Fig. 2a). Histological analysis confirmed that ablation significantly reduced the number of Vgat$^+$ neurons in the MeApd (Fig. 2b,c). Although most control animals developed a consistent preference for the social port, a lower proportion of animals with MeApd Vgat$^+$ neurons ablated developed such preference (Fig. 2d). Vgat$^+$ neuron-ablated animals showed no significant preference for the social port and no increase in the numbers of pokes in the social port compared to control (Fig. 2e–h and Extended Data Fig. 3a,b). These results suggest that MeApd Vgat$^+$ neurons are required for social reward behavior.

To test whether MeApd Vgat$^+$ neurons are also required for the preference for the social port after training, we acutely suppressed the activity of Vgat$^+$ neurons after animals developed their preference for the social port using a Cre-dependent silencing opsin GtACR (Fig. 2i,j). Efficient photostimulation-dependent silencing of GtACR-expressing Vgat$^+$ neurons was confirmed by electrophysiological recordings in acute brain slices (Extended Data Fig. 3c,d). In the social operant task, silencing of Vgat$^+$ neurons led to an acute suppression of pokes in the social port, suggesting that MeApd Vgat$^+$ neurons are also required for processing social reward after training (Fig. 2k,l). In addition, we found that suppressing MeApd Vgat$^+$ neuron activity also reduced the time that subject animals spent on close social investigation of juvenile mice in free social interactions (Extended Data Fig. 3e–h).

To further determine whether MeApd Vgat$^+$ neurons are active specifically during social reward, we recorded their neuronal dynamics during the presentation of social versus non-social natural rewarding stimuli (such as chocolate and sucrose solution). We found that Vgat$^+$ neurons responded to social stimuli but not other naturally rewarding stimuli (Extended Data Fig. 4a,b). Moreover, we found that caspase-3-mediated ablation of MeApd Vgat$^+$ neurons did not impair the animals' positive preference for food reward (Extended Data Fig. 5a–d). These results suggest that the MeApd is likely specifically involved in social reward.

Activating MeApd Vgat$^+$ neurons promotes reinforcement behavior. The above results suggest that activity of MeApd Vgat$^+$ neurons might represent positive social signals. If the MeA transforms social cues into reward signals, we hypothesize that direct activation of MeA neurons might bypass the requirement of upstream social inputs and should be sufficient to produce a rewarding experience and drive reinforcement. To determine if activation of Vgat$^+$ neurons promotes reinforcement, we expressed a Cre-dependent activating opsin ChR2 (or EYFP as a control) in the MeApd of Vgat-Cre animals (Fig. 3a,b). Using the real-time place preference (RTPP) assay as a measure for reinforcement behavior, we found that animals developed a consistent positive preference for the

Fig. 1 | Adult mice exhibit robust reinforcement for social reward in an automated operant task. a,**b**, Diagram illustrating an automated social operant task and the experimental pipeline. **c**,**f**, An animal (right) can freely nose-poke the social port, which automatically triggers the opening of a retractable gate after a 3-s delay. The mouse is then allowed to closely interact for 7 s with an unfamiliar juvenile animal (**c**) or with an empty social chamber (**f**). Poking the null port causes a 10-s timeout before the next trial starts. Gate opening and closure takes 2 s to complete. **d**,**g**, Representative raster plots showing nose-pokes of social and null ports before (day 0) and after (day 7) training, with the presence (**d**) or absence (**g**) of target animals. **e**,**h**, Cumulative distribution of nose-pokes in social and null ports from examples shown in **d** and **g**, on days 0 and 7. **i**, Subject animals develop a strong preference for the social port (calculated as the difference in the percentage of nose-pokes between social and null ports) with the presence of target animals over a 10-d experiment (1 d of baseline session, 7 d of training sessions with target animals and 2 d of post-training sessions without target animals). One-way repeated-measures ANOVA with Bonferroni post hoc correction ($^*P < 0.05$, $^{***}P < 0.001$). **j**, Number of pokes of social and null ports with target animals across 10 d. Two-way repeated-measures ANOVA with Bonferroni post hoc correction ($^{**}P < 0.01$, $^{***}P < 0.001$). **k**, Subject animals fail to develop a preference for the empty social port without target animals over an 8-d experiment (1 d of baseline session and 7 d of training sessions with an empty social chamber). As the animals did not develop any preference for the empty social port, no post-training session was performed. $P = 0.1227$, one-way repeated-measures ANOVA. **l**, Number of pokes of null and empty social ports across 8 d. $P = 0.1216$, two-way repeated-measures ANOVA. **m**–**p**, Subject animals display distinct behavioral characteristics on the first (day 1) and last (day 7) days of the training session—fractions of trials showing anticipatory behavior (**m**), duration of anticipatory behavior (**n**), duration of interactions with the target animal during the 7-s interaction window (**o**) and latency to first social contact after the gate opens (in trials when the subject pokes the social port) (**p**). Two-way repeated-measures ANOVA with Bonferroni post hoc correction ($^*P < 0.05$, $^{***}P < 0.001$). In **i**, **j** and **m**–**p**, $n = 17$ mice; in **k** and **l**, $n = 25$ mice. **i**–**l**, mean ± s.e.m.; **m**–**p**, box plots: center = median, box = quartiles, whiskers = 10th and 90th percentiles. For detailed statistical information, see Supplementary Table 1.

chamber coupled with stimulation (Fig. 3c–e). Consistently, in the intracranial self-stimulation assay, animals developed a positive preference to self-stimulate their Vgat⁺ neurons compared to poking a null port (Fig. 3f–h and Extended Data Fig. 6a). To determine whether the MeApd-mediated reward is specific to a particular sex, we examined the effect of activating the MeApd Vgat⁺ neurons in both male and female mice. We found that activating these neurons produced a similarly strong preference for stimulation in both sexes, in both the RTPP assay and the intracranial self-stimulation assay (Extended Data Fig. 6b–g). These results suggest that activation of MeApd Vgat⁺ neurons is, indeed, highly rewarding in both males and females. The finding that activating these neurons can drive reinforcement independent of a social context does not mean that these neurons are non-specifically involved in general reward but

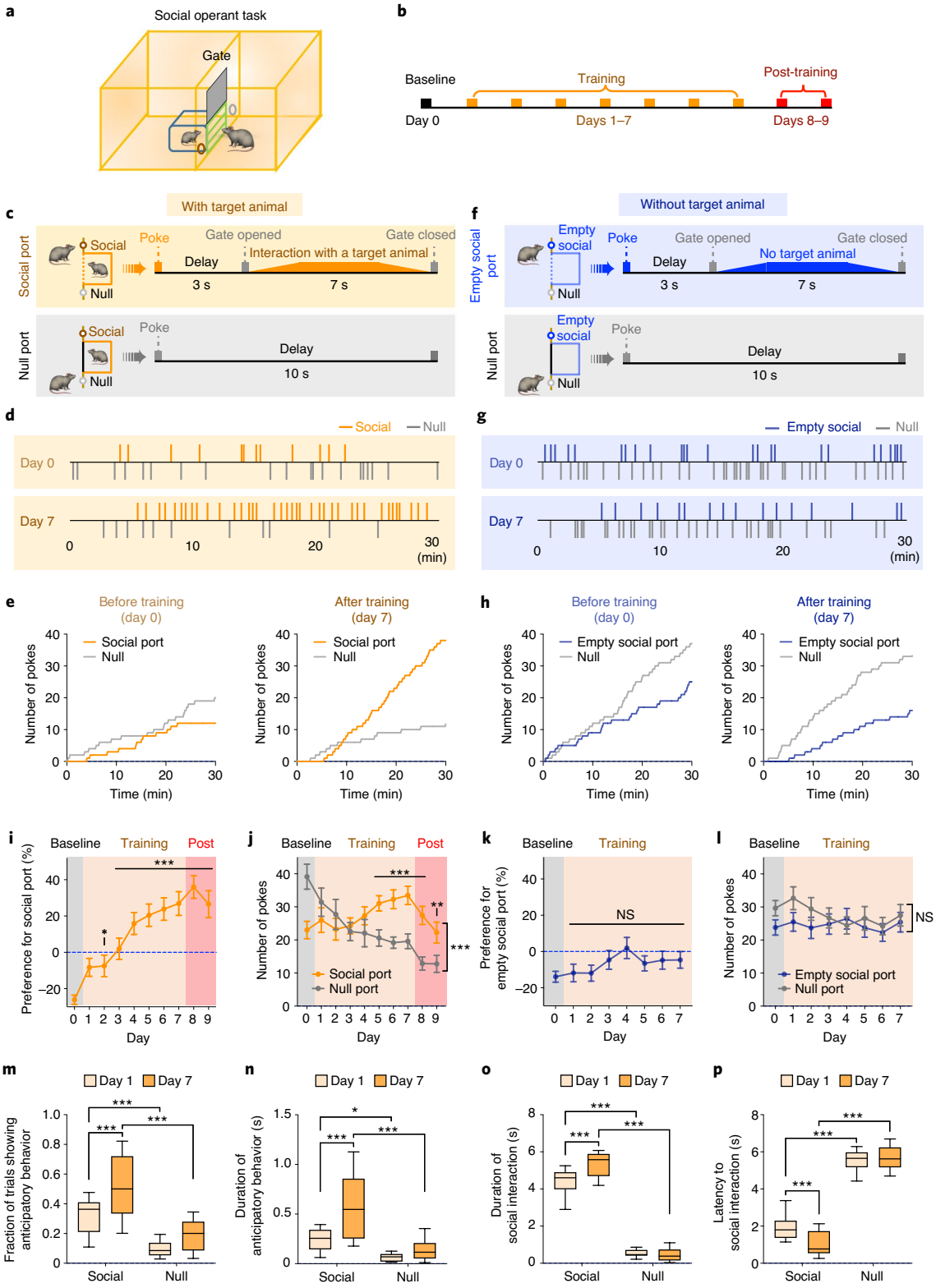

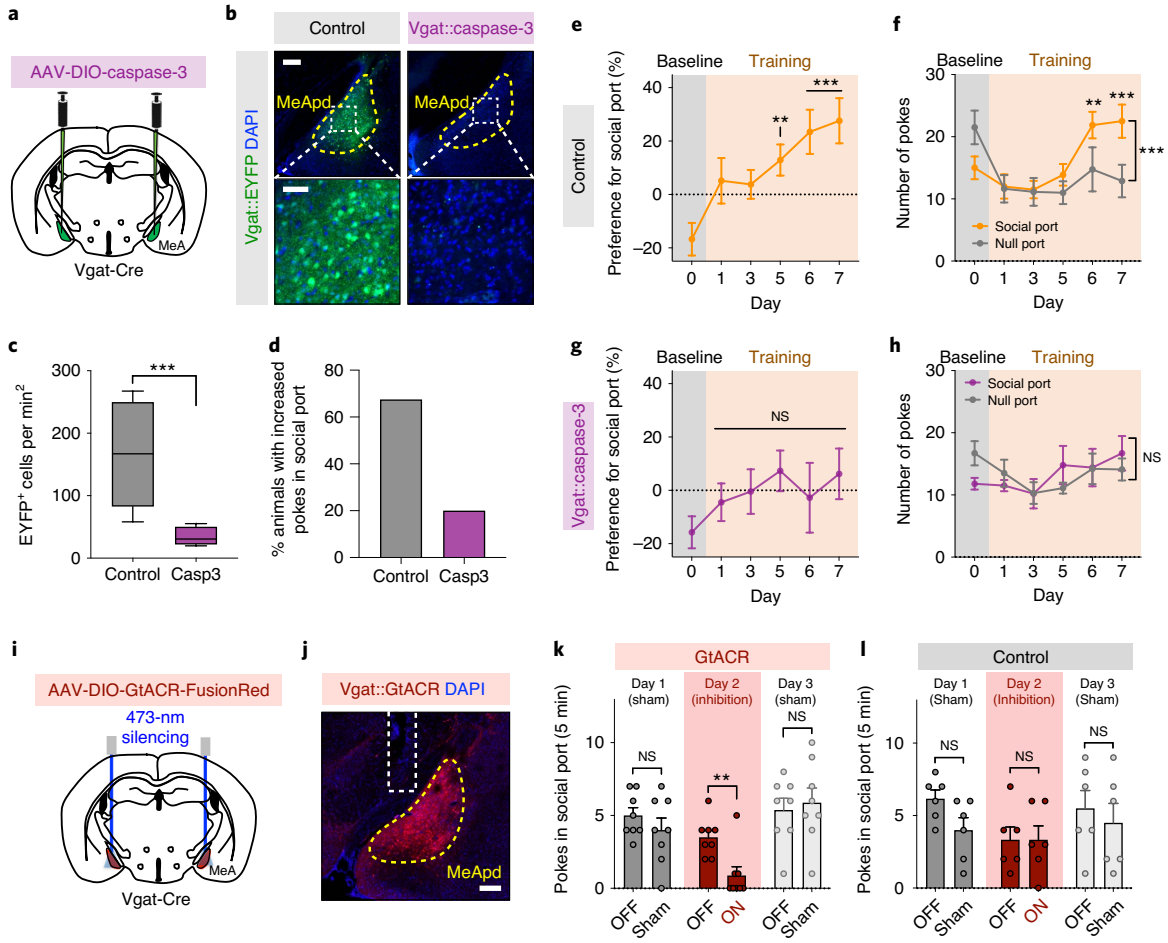

Fig. 2 | MeApd Vgat⁺ neurons are required for social reward. a, Schematic of viral injection for cell-type-specific ablation. **b**, Representative images of MeApd Vgat⁺ neurons (labeled by EYFP) in control and caspase-3-expressing animals. Top images: scale bar, 200 μm; bottom images: scale bar, 50 μm. **c**, Quantification of EYFP-expressing Vgat⁺ neurons in control and caspase-3-expressing animals. Cell-type-specific ablation substantially reduced Vgat⁺ neurons in the MeApd. ***$P < 0.0001$, Mann–Whitney test (two sided). **d**, Fractions of animals that exhibit a consistent preference for the social port in control or caspase-3-expressing animals. **e**,**g**, Caspase-3-expressing animals (**g**), but not controls (**e**), fail to develop a preference for the social port during the training session. One-way repeated-measures ANOVA with Bonferroni post hoc correction (**$P < 0.01$, ***$P < 0.001$). **f**,**h**, Number of pokes of social and null ports with target animals across days. Two-way repeated-measures ANOVA with Bonferroni post hoc correction (**$P < 0.01$, ***$P < 0.001$). **i**, Schematic of viral injection for optogenetic inhibition. **j**, A representative image showing the expression of GtACR-FusionRed in MeApd Vgat⁺ neurons. Scale bar, 200 μm. **k**,**l**, Optogenetic silencing of MeApd Vgat⁺ neurons in GtACR-expressing (**k**) but not control (**l**) animals significantly reduces pokes in the social port in the social operant task. After animals established a positive preference for the social port, sham inhibition was performed on days 1 and 3, whereas optogenetic inhibition was performed on day 2. In **b**–**h**, $n = 10$ mice (caspase-3) and 8 mice (control). In **j**–**l**, $n = 8$ mice (GtACR) and 6 mice (control). Two-way repeated-measures ANOVA with Bonferroni post hoc correction (**$P < 0.01$). **c**, Box plots: center = median, box = quartiles, whiskers = 10th and 90th percentiles; **e**–**h**, **k**, **l**, mean ± s.e.m. For detailed statistical information, see Supplementary Table 1.

likely reflects an induced gain of function that is sufficient to bypass upstream social inputs.

The observation that the MeApd generates reward raised the possibility that the activity of MeApd Vgat⁺ neurons is sufficient to drive positive reinforcement over days. We used a paradigm that mimicked our social operant task, where the 'social' port is coupled with optogenetic stimulation of MeApd Vgat⁺ neurons in place of presentation of target animals (Fig. 3i). We found that, over 3 d of training, animals developed a strong preference for and increased numbers of pokes toward the optogenetic port (Fig. 3j–m and Extended Data Fig. 7a,b,e,f), suggesting that activating MeApd Vgat⁺ neurons is, indeed, sufficient to drive positive reinforcement over days.

We next asked whether reward is specifically regulated by Vgat⁺ neurons in the MeApd. The MeApd consists of both Vgat⁺ and Vglut2⁺ neurons[12]. We found that activating Vglut2⁺ neurons in the RTPP assay did not promote any positive preference in the stimulated chamber but, rather, caused the animals to spend significantly less time there (Extended Data Fig. 8), suggesting that Vglut2⁺ neuron activity is associated with a negative valence. This result further suggests that the positive reinforcement is specifically controlled by Vgat⁺ neurons.

Activation of MeApd Vgat⁺ neurons drives dopamine release. Release of dopamine is a characteristic associated with rewarding experiences[5,32,33]. Our results raise an important question of whether the MeApd might regulate the dopamine reward system. Using a genetically encoded fluorescent dopamine sensor (dLight), we first examined the patterns of dopamine signals in the NAc when animals were exposed to various social stimuli. We injected an adeno-associated virus (AAV) that expresses dLight (or EYFP as a

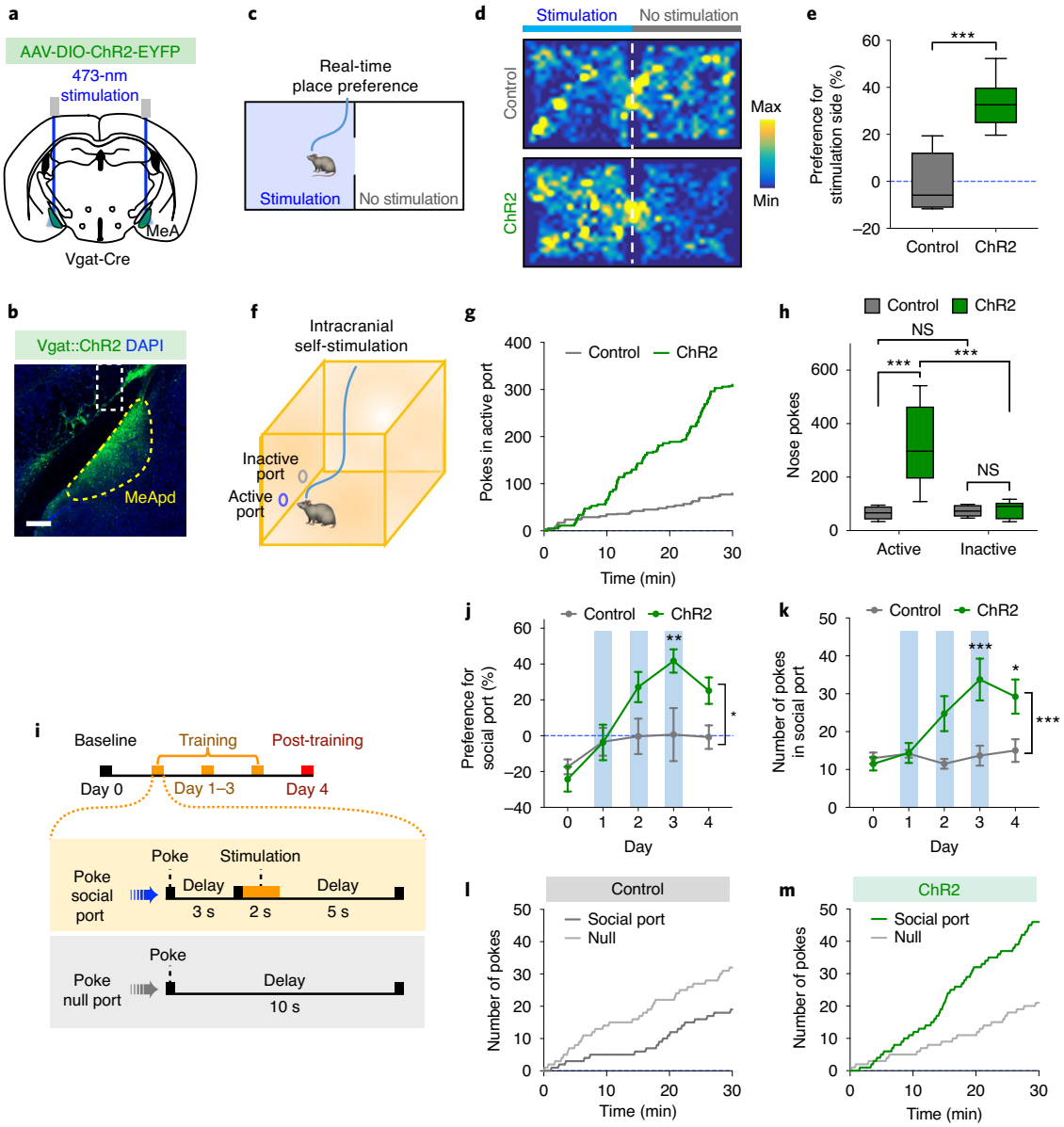

Fig. 3 | Activation of MeApd Vgat⁺ neurons is sufficient to drive reinforcement. a, Schematic showing viral injection and fiber implantation for optogenetic activation of MeApd Vgat⁺ neurons. **b**, Example image of injection site and viral expression in the MeApd of Vgat-Cre animals. Scale bar, 200 µm. **c**, Schematic showing RTPP assay. Light blue area indicates the chamber paired with light stimulation when the animal enters. **d**, Representative heat maps showing locomotion trajectories of control (top) and ChR2-experessing (bottom) mice in the RTPP test. **e**, ChR2-expressing animals display a significant preference for the stimulation-coupled chamber compared to EYFP-expressing controls. ***$P < 0.001$, Mann–Whitney test (two sided). **f**, Schematic showing an intracranial self-stimulation assay. The active port is coupled with optogenetic stimulation. **g**, Cumulative distribution of the number of nose-pokes in the active port by a representative ChR2-expressing or control animal in the self-stimulation assay. **h**, ChR2-expressing animals exhibit a greater number of pokes in the active port, whereas control animals do not. Two-way repeated-measures ANOVA with Bonferroni post hoc correction (***$P < 0.001$). **i**, Schematic showing a modified social operant task, where presentation of target animals is replaced with 2-s optogenetic stimulation of the MeApd Vgat⁺ neurons. Poking the optogenetic social port leads to a 3-s delay followed by a 2-s stimulation, whereas poking the null port leads to a timeout with no stimulation. The 5-d experiment consists of 1 d of baseline session, 3 d of training sessions and 1 d of post-training session. **j**,**k**, ChR2-expressing animals develop a strong preference (**j**) for and increased nose-pokes (**k**) in the optogenetic social port over 3 d of training, whereas control animals do not. Two-way repeated-measures ANOVA with Bonferroni post hoc correction (*$P < 0.05$, **$P < 0.01$, ***$P < 0.001$). **l**,**m**, Cumulative distribution of the numbers of pokes in control (**l**) and ChR2-expressing (**m**) mice on day 3 of training. In **b**–**e**, $n = 16$ mice (ChR2) and $n = 6$ mice (control); in **g** and **h**, $n = 10$ mice (ChR2) and $n = 6$ mice (control); in **j** and **k**, $n = 8$ mice (ChR2) and $n = 6$ mice (control). **e**,**h**, Box plots: center = median, box = quartiles, whiskers = 10th and 90th percentiles; **j**,**k**, mean ± s.e.m. For detailed statistical information, see Supplementary Table 1.

control) into the NAc and examined dopamine signals by measuring dLight fluorescence in awake animals using fiber photometry (Fig. 4a,b). We observed a significant increase in dopamine signals when subject animals freely interacted with males, females or juvenile animals (Fig. 4c–f), suggesting that social interactions induce a robust increase of dopamine signals in the NAc.

We then recorded dLight fluorescence in the NAc while animals performed the social operant task (Fig. 4g–s). We observed

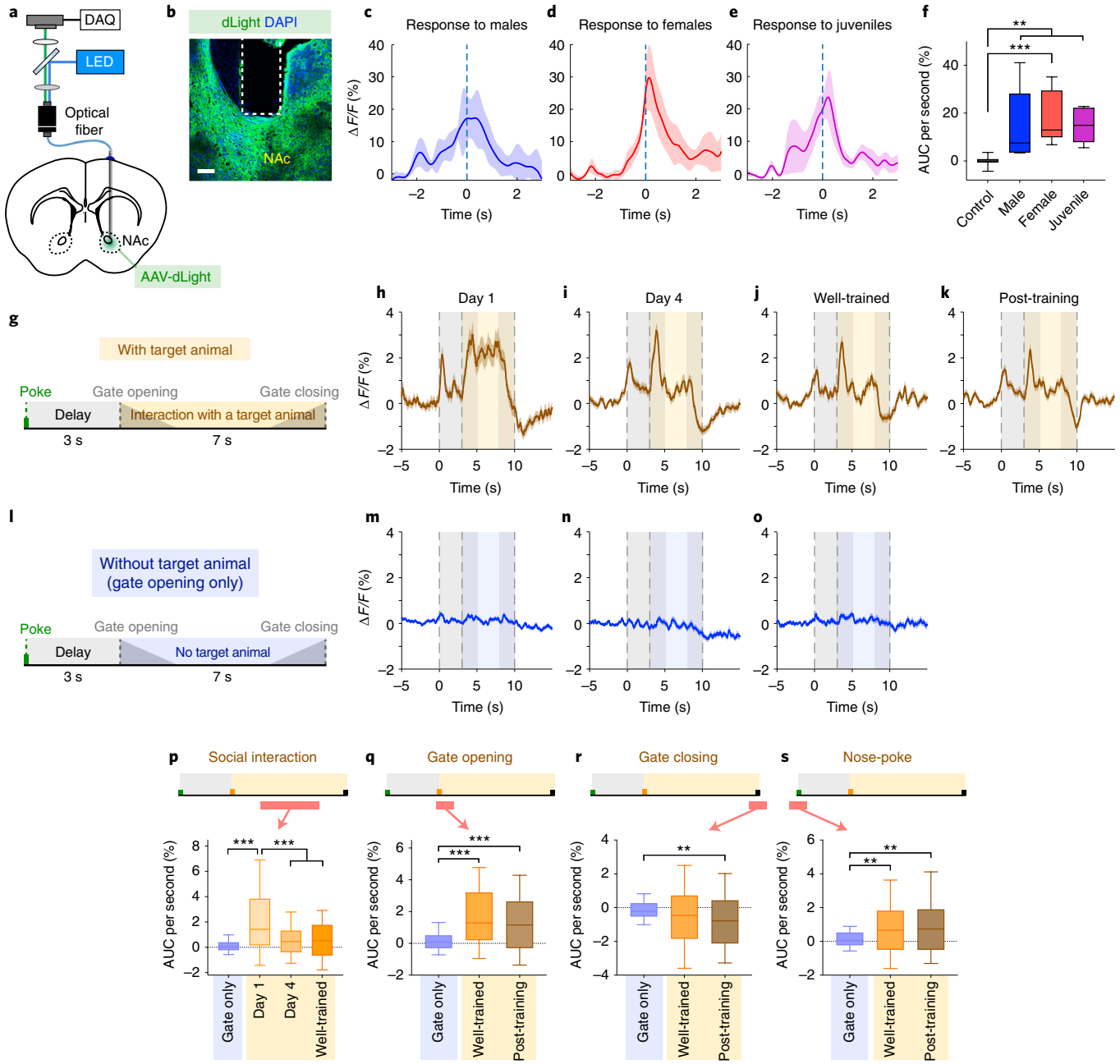

Fig. 4 | Dynamics of dopamine signals in the NAc during social operant task. a, Schematic showing fiber photometry for measuring dopamine signals in the NAc using the fluorescent dopamine sensor dLight. DAQ, data aquisition system. **b**, Example image showing dLight expression and fiber placement in the NAc. Scale bar, 100 µm. **c**–**e**, dLight fluorescence changes in response to males (**c**), females (**d**) or juveniles (**e**). **f**, AUC per second during different social stimuli. Kruskal–Wallis test (one-way ANOVA on ranks) with Dunn's post hoc correction (**$P<0.01$, ***$P<0.001$). **g**–**s**, Dynamics of dLight fluorescence in the NAc during the social operant task. **g**,**l**, Schematic showing the social operant task in the presence (**g**) or absence (**l**) of target animals. Gate opening (3–5 s) and closure (8–10 s) takes 2 s to complete. **h**–**k**, dLight fluorescence changes in subject animals trained in the social operant task with target animals at different training stages: day 1 (**h**), day 4 (**i**), well trained (**j**) and post-training test (**k**). **m**–**o**, dLight fluorescence changes in subject animals trained without target animals on day 1 (**m**), day 4 (**n**) and day 7 (**o**). **p**–**s**, AUC per second at different periods within single operant trials: during social interaction (5–8 s, **p**), during gate opening (3–4 s, **q**), at gate closing (9.5–10.5 s, **r**) and at nose-poking (−0.5–1.5 s, **s**). Kruskal–Wallis test with Dunn's post hoc correction (** $P<0.01$, ***$P<0.001$). In **c**–**f**, $n=15$ trials from four control mice and $n=6$ trials (for each behavior) from three dLight mice. In **p**, $n=108$ trials from seven mice (without target animal, day 1), $n=96$ trials (day 1), $n=177$ trials (day 4) and $n=249$ trials (well trained) from seven mice. In **q**–**s**, $n=92$ trials from 7 mice (without target animal, day 7), $n=249$ trials (well trained) and $n=305$ trials (post-training) from 7 mice with target animal. **c**–**e**, **h**–**k** and **m**–**o**, mean ± s.e.m.; **f** and **p**–**s**, box plots: center = median, box = quartiles, whiskers = 10th and 90th percentiles. For detailed statistical information, see Supplementary Table 1.

a significant increase in dopamine signal during the social interaction period. The signal was highest in the initial phase of training and was reduced when the animals were well trained (Fig. 4p). Interestingly, an elevated signal was observed immediately after gate opening, which signals the onset of social interaction (Fig. 4q). This increase remained when the animals were well trained and

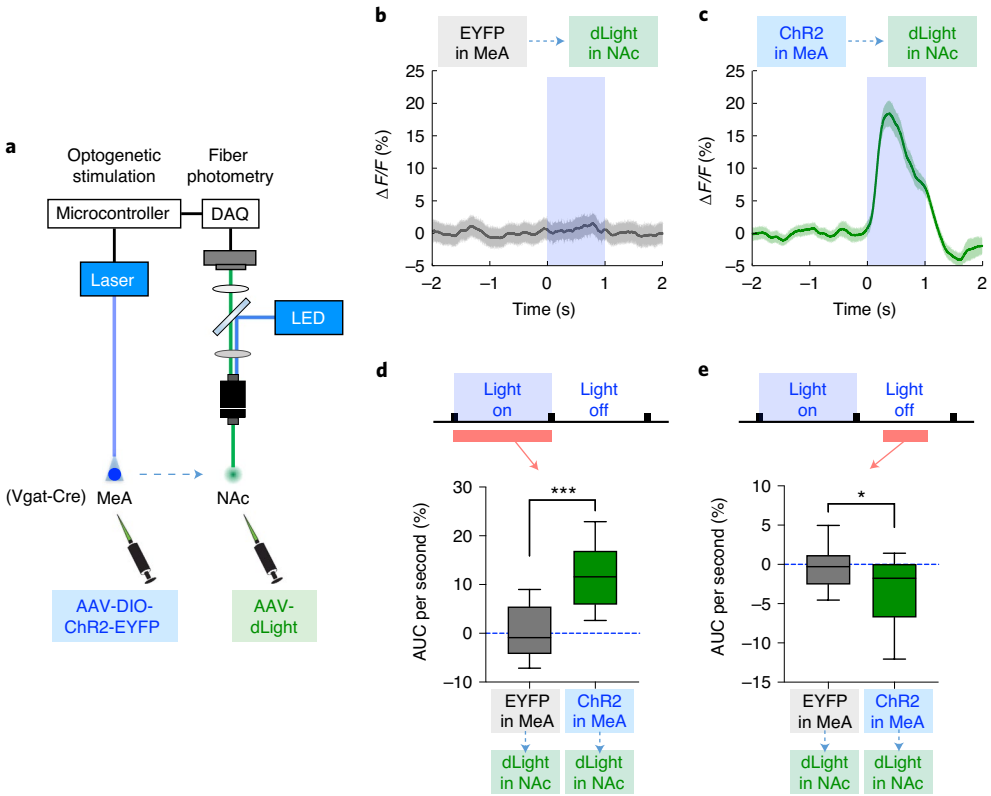

Fig. 5 | Activating MeApd Vgat⁺ neurons triggers dopamine release in the NAc. a, Schematic showing fiber photometry for measuring dopamine signals in the NAc using dLight fluorescence while optogenetically activating MeApd Vgat⁺ neurons. **b**,**c**, dLight fluorescence changes in the NAc in response to 1-s optogenetic stimulation of the MeApd in EYFP (**b**) or ChR2-expressing (**c**) mice. **d**, AUC per second during optogenetic stimulations (0–1 s from the onset). ***$P < 0.001$, Mann–Whitney test (two sided). **e**, AUC per second after optogenetic stimulations (0.3–0.6 s from the offset). *$P = 0.0125$, Mann–Whitney test (two sided). In **b**–**e**, $n = 56$ trials for controls from six mice and $n = 39$ trials for ChR2 from four mice. **b**,**c**, Mean ± s.e.m.; **d**,**e**, box plots: center = median, box = quartiles, whiskers = 10th and 90th percentiles. For detailed statistical information, see Supplementary Table 1.

even during the post-training test in the absence of target animals, suggesting that dopamine release is associated with this conditional cue, signaling the onset of social interaction. By contrast, at the end of the social interaction period, dLight signal dropped significantly when the gate started to close at 8 s, which reflects the removal of social reward (Fig. 4r). Finally, nose-poke actions were also associated with an increase of dLight signal (Fig. 4s), which might indicate that the elevation in motivation to nose-poke for social reward is associated with elevated dopamine release. Notably, all of these dLight signals were not observed or were significantly weaker when animals were trained with gate opening alone (without target animals), confirming that the observed changes of dopamine signals are, indeed, related to social reward rather than simply due to gate opening or closure alone. Collectively, these results suggest that changes of dopamine signals in the NAc are associated with the rewarding social interaction and triggered by related cues.

We next asked whether activating MeApd Vgat⁺ neurons is sufficient to induce dopamine release in the NAc. To this end, we injected an AAV expressing Cre-dependent ChR2 into the MeApd of Vgat-Cre animals and injected another AAV expressing dLight into the NAc of the same animals (Fig. 5a). We then measured dLight fluorescence in awake animals using fiber photometry while optogenetically activating MeApd Vgat⁺ neurons. Strikingly, we found that ChR2 activation of Vgat⁺ neurons triggered a robust, time-locked increase of dLight fluorescence in the NAc, whereas photostimulation of EYFP-expressing control animals did not have this effect (Fig. 5b–d). After the offset of stimulation, the dLight signal showed a significant reduction (Fig. 5e), which likely reflects the termination of optogenetically induced reward. These results demonstrate that activation of MeApd Vgat⁺ neurons is sufficient to drive robust, time-locked dopamine release.

MPOA-projecting MeApd neurons mediate social reward behavior. As the MeA does not directly project to classic reward centers, such as the NAc, an important question is how the MeApd processes reward through downstream circuitry. Given that the MeApd projects to the medial preoptic nucleus that directly connects to the VTA[11,34,35], the MeApd-to-MPOA pathway is an attractive candidate for mediation of social reward.

To test this, we injected an AAV expressing Cre-dependent ChR2 (or EYFP as a control) in the MeApd and implanted optic fibers above the MPOA to specifically activate the axonal terminals of MeApd Vgat⁺ neurons that directly project to the MPOA (Fig. 6a,b). Indeed, activating these axonal terminals in the MPOA produced a strong positive preference in both the RTPP test and the intracranial self-stimulation test (Fig. 6c–f and Extended Data Fig. 7i), suggesting that MPOA-projecting terminals carry reinforcement signals. To determine whether activation of the MeApd-to-MPOA circuit is also sufficient to drive reinforcement behavior over days, we tested these animals in a test similar to that in Fig. 3 (Fig. 6g) and found that activating MPOA-projecting terminals was able to generate a strong preference for and increased numbers of pokes toward the optogenetic port over days (Fig. 6h,i and Extended Data Fig. 7c,d,g,h). These results suggest that activation of the MeApd-to-MPOA circuit is, indeed, sufficient to promote reinforcement behavior.

To further determine whether the reinforcement behavior is specifically driven by the MeApd-to-MPOA circuit, we first ruled out the possibility that this reinforcement behavior is caused by antidromic activation of collateral projections to other brain areas. To prevent backpropagating action potentials from spreading to other collateral projections, we locally infused lidocaine into the MeApd while activating axonal projections in the MPOA (Extended Data Fig. 9a,b). We found that blocking backpropagating action potentials did not affect the behavioral function of stimulating the MeApd-to-MPOA projection (Extended Data Fig. 9b), suggesting that this behavioral effect is, indeed, caused by the MeApd-to-MPOA projection but not by other collateral branches. Furthermore, we directly manipulated another major axonal target of MeApd Vgat$^+$ neurons in the ventral premammillary nucleus (PMV) in ChR2-expressing animals and found that photostimulation of axonal projections to the PMV did not promote reinforcement behavior (Extended Data Fig. 9c,d). Together, these results strongly suggest that the MPOA projection of MeApd Vgat$^+$ neurons is specifically involved in processing social reward and reinforcement.

To test whether the MeApd-to-MPOA circuit is also required for the preference for the social port in the social operant task, we acutely suppressed the activity of MPOA-projecting MeApd neurons after animals developed their preference for the social port. To specifically label MeApd neurons that project to the MPOA, we injected a retrograde AAV expressing Cre recombinase into the MPOA and a second AAV expressing Cre-dependent GtACR into the MeApd (Fig. 6j–l). Similarly to what was observed when silencing all MeApd Vgat$^+$ neurons, silencing MPOA-projecting MeApd neurons by GtACR also led to an acute suppression of pokes in the social port. These results suggest that MPOA-projecting MeApd neurons are also required for processing social reward (Fig. 6m,n).

We found that, among MeApd neurons that project to the MPOA, 85.3% are GABAergic (Extended Data Fig. 10a–e). To rule out the possibility that MPOA-projecting glutamatergic neurons might also contribute to reinforcement behavior, we specifically activated the axonal projections of MeApd glutamatergic neurons in the MPOA using optogenetics (Extended Data Fig. 10f,g). We found that activating glutamatergic projections to the MPOA does not promote any positive reinforcement.

To further determine whether the MeApd-to-MPOA circuit is also selective for social reward, we expressed axon-localized GCaMP6 in MeApd Vgat$^+$ neurons and used fiber photometry to record calcium activity in their axonal projections in the MPOA during exposure to social and non-social stimuli (Extended Data Fig. 4c,d). We found that, similarly to MeApd Vgat$^+$ neurons themselves, axonal projections to the MPOA also displayed strong responses during social interaction but little response to food reward (Extended Data Fig. 4c,d). Furthermore, ablating MPOA-projecting MeApd neurons did not impair the animals' preference for food reward (Extended Data Fig. 5e–h). These results suggest that MPOA-projecting MeApd neurons are not directly involved in promoting food reward.

MeApd-mediated reward overcomes avoidance behavior. Positive social interaction can buffer against aversive experiences[2,36], but the underlying mechanism at the circuit level has been largely unclear. The observation that the MeApd circuit mediates social reward offers an opportunity to ask whether positive signals mediated by the MeApd circuit can overcome negative experiences and suppress the associated behaviors with negative valence. Animals typically display a robust avoidance behavior to move away from locations associated with negative valence. In a large open field, mice innately prefer to stay in the periphery of the arena, as the center is associated with potential danger. When we coupled optogenetic stimulation to the center area (Fig. 7a–c), ChR2-expressing animals spent substantially longer time in the center, whereas control animals did not show this increase (Fig. 7d,e). This suggests that the rewarding effect of activating these neurons is sufficiently strong to act against the innate avoidance of the central area.

Similarly, in an elevated plus maze, animals innately prefer to stay in closed arms and spend much less time in open arms that are associated with a negative valence. When we coupled optogenetic stimulation to open arms, the animals spent substantially longer time in those areas (Fig. 7i–m), suggesting that the rewarding effect of activating MeApd Vgat$^+$ neurons similarly overcomes the innate avoidance of open arms.

Finally, we examined whether this effect is also mediated by the MeApd–MPOA circuit by specifically activating the MeApd Vgat$^+$ axonal terminals in the MPOA (Fig. 7f). When coupling optogenetic activation to the center area in the open field or open arms in the elevated plus maze, we observed a similar increase of time spent in these areas that are associated with negative valence (Fig. 7f–h,n–p). This suggests that activation of the MeApd–MPOA pathway is sufficient to mediate this effect. Together, these results establish a key role for the MeA-to-MPOA circuit in generating positive signals that can overcome avoidance behavior.

Fig. 6 | The MPOA-projecting MeApd circuit mediates social reward. a, Schematic showing viral injection and fiber placement for optogenetic activation of axonal terminals of MeApd Vgat$^+$ neurons in the MPOA. **b**, Example image showing projections of MeApd Vgat$^+$ neurons in the MPOA. Scale bar, 200 μm. **c**, Representative heat maps showing locomotion trajectories of control and ChR2-experessing mice in the RTPP test. **d**, ChR2-expressing animals with axonal terminals stimulated display a positive preference for the stimulation-coupled chamber compared to EYFP controls. $^{**}P < 0.0025$, Mann–Whitney test (two sided). **e**, Cumulative distribution of the number of nose-pokes in the active port by a representative ChR2-expressing or control animal during the self-stimulation assay. **f**, ChR2-expressing animals with axonal terminals stimulated exhibit a greater number of pokes in the active port, whereas control animals do not. Two-way repeated-measures ANOVA with Bonferroni post hoc correction ($^{***}P < 0.001$). **g**, Schematic showing a modified social operant task, where presentation of target animals is replaced with 2-s optogenetic stimulation of Vgat$^+$ neuron terminals in the MPOA. As in Fig. 3i, poking the optogenetic social port leads to a 3-s delay followed by a 2-s stimulation. The 5-d experiment consists of 1 d of a baseline session, 3 d of training sessions and 1 d of a post-training session. **h**,**i**, ChR2-expressing animals develop a strong preference (**h**) for and increased nose-pokes (**i**) in the optogenetic social port over 3 d of training, whereas control animals do not. Two-way repeated-measures ANOVA with Bonferroni post hoc correction ($^{*}P < 0.05$, $^{**}P < 0.01$, $^{***}P < 0.001$). **j**, Schematic showing viral injection and fiber placement for optogenetic inhibition of MPOA-projecting MeApd neurons. **k**,**l**, Example image showing the expression of AAV-retro-EGFP-Cre in the MPOA (**k**) and GtACR in the MPOA-projecting MeApd neurons (**l**). Blue, DAPI; green, EGFP; red, GtACR-FusionRed. Scale bar, 200 μm. **m**,**n**, Optogenetic inhibition of neural activity in GtACR-expressing (**m**) but not control (**n**) mice reduces pokes in the social port in the social operant task (Methods). After animals established a positive preference for the social port, sham inhibition was performed on days 1 and 3, whereas optogenetic inhibition was performed on day 2. Two-way repeated-measures ANOVA with Bonferroni post hoc correction ($^{**}P < 0.01$). Silencing MPOA-projecting MeApd neurons also reduces social preference in the three-chamber assay (Extended Data Fig. 9e–g). In **c** and **d**, $n = 7$ mice (ChR2) and 5 mice (control); in **e** and **f**, $n = 7$ mice (ChR2) and 5 mice (control); in **h** and **i**, $n = 8$ mice (ChR2) and 8 mice (control); in **m** and **n**, $n = 8$ mice (GtACR) and 4 mice (control). **d**,**f**, Box plots: center = median, box = quartiles, whiskers = 10th and 90th percentiles. **h**,**i**,**m**,**n**, mean ± s.e.m. For detailed statistical information, see Supplementary Table 1.

Discussion

Using an automated social operant task to measure social reward in mice, we show that adult mice, both male and female, are capable of developing positive reinforcement associated with social reward. Using this assay, we uncovered a previously unknown role for the MeA in regulating social reward. We found that Vgat$^+$ neurons in the MeApd are required for social reward behavior, and activating these neurons drive positive reinforcement. We show that dopamine signals in the NAc are associated with social reward-related cues during the social operant task and that activation of MeApd Vgat$^+$ neurons promotes dopamine release in the NAc. Finally, the rewarding effect produced by MeApd Vgat$^+$ neurons is mediated by their projections to the MPOA and is strong enough to overcome avoidance behavior. Together, these results establish a direct causal

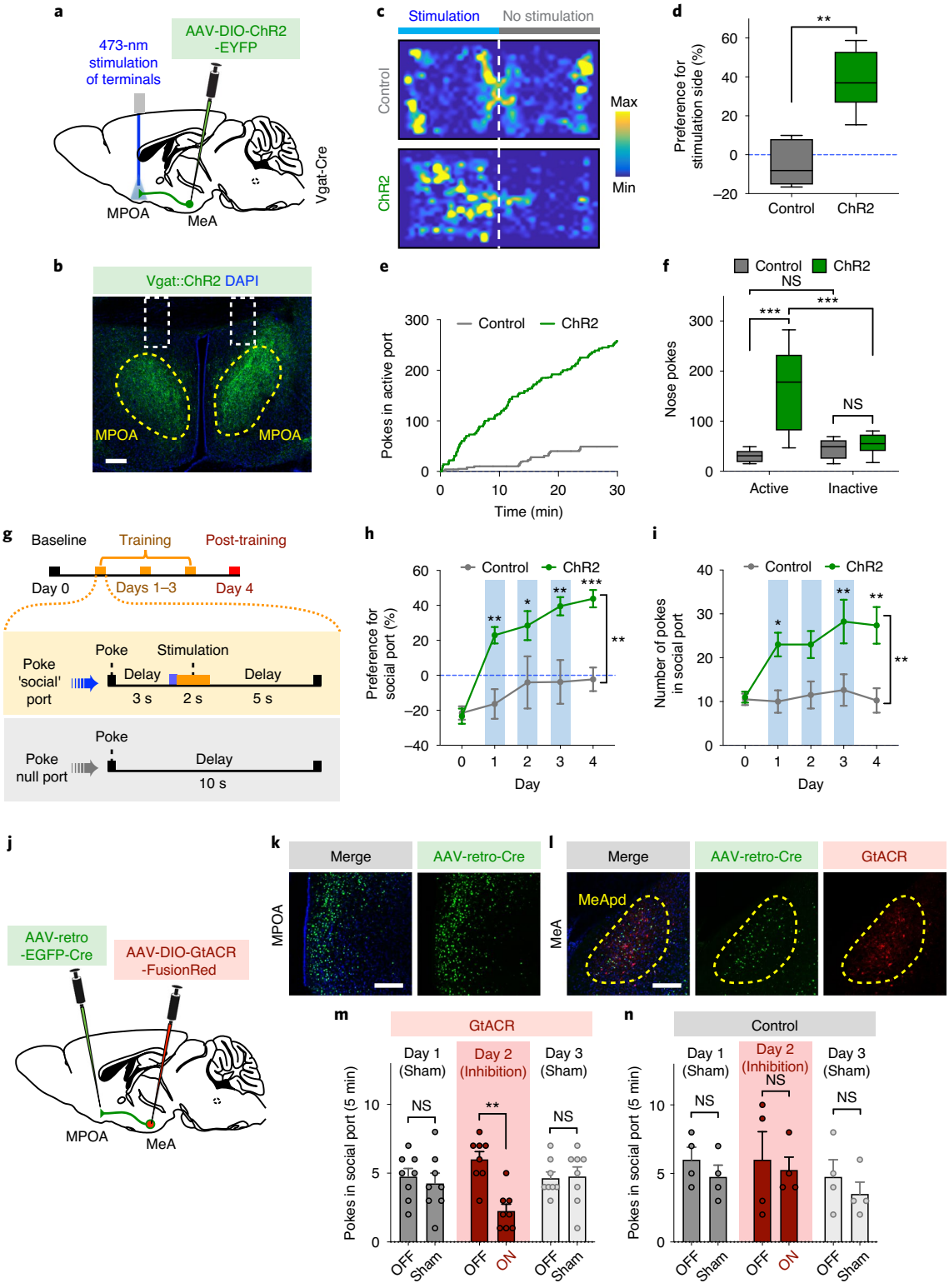

role for MeA Vgat$^+$ neurons in mediating social reward behavior and present a mechanism for controlling social reward beyond the classical reward system.

Previous studies using the social conditioned place preference assay suggest that juvenile, but not adult, mice are able to establish a persistent social reward preference[37]. We developed a fully automated operant conditioning system in which animals are trained to nose-poke specific ports to engage in social interactions. Using this system, we present conclusive evidence that adult mice of both sexes exhibit robust preference for social reward, demonstrating that our assay is effective at measuring social reward in adult animals. As this system is fully automated, it increases efficiency and minimizes unnecessary manual disturbance during experiments. The inclusion of a barrier allows us to specifically examine motivation and rewarding effect of behavior initiated by the subject animal, as opposed to passive experiences of behavior initiated by target animals. Although animals are able to receive and recognize social cues through the wire grid barrier (such as olfactory, visual or auditory signals) and can engage in social approach and close social investigation, the presence of a barrier does not allow us to examine full interactions between animals that involve physical contact. As a complementary approach, we also examined social interactions in a freely moving context before performing social operant tasks and showed that adult animals predominantly engaged in close investigation behavior toward juvenile animals.

Although reward processing for non-social stimuli has been studied extensively, less is known about the brain regions that mediate social reward[5]. Previous studies largely focused on brain regions in the classic mesolimbic reward system, such as the NAc and the VTA, and brain regions that directly connect to them[8–11]. A common picture from these studies is that the same circuitry that processes non-social reward signals also processes social reward[9,10,37]. Indeed, we found that, in the social operant task, dopamine release in the NAc was significantly elevated during social interaction as well as during gate opening (as a conditioned cue signaling the onset of social interaction), consistent with the role of dopamine during appetitive food- or drug-seeking behavior[32,33,38,39] and during a similar social reward behavior in a recent preprint[40].

Although MeApd was previously implicated in several social behaviors in a sex- and behavioral context-dependent manner[12,13,23–26], whether it is involved in mediating positive reinforcement of social interaction was unclear. Here we provide multiple lines of evidence that clearly establish the MeApd as a new circuit component in regulating social reward. The activity of MeApd Vgat$^+$ neurons is required for processing social reward and is sufficient to drive reinforcement behavior. Our finding that activating these neurons can drive reinforcement does not mean that these neurons are non-specifically involved in general reward but, rather, reflects a gain of function that is sufficient to bypass the requirement of social cues. Indeed, the activity of MeApd Vgat$^+$ neurons is not required for mediating food reward, and activation of Npy1r$^+$ neurons in the MeA can suppress feeding behavior[41]. Although we cannot exclude the possibility that these neurons are involved in other types of reward that we did not examine, our data suggest that the MeApd is unlikely non-specifically involved in processing all appetitive stimuli. Interestingly, activation of MeApd Vgat$^+$ neurons drives the release of dopamine in the NAc, which suggests that, although the MeApd is not part of the classic mesolimbic system, positive social signals mediated by MeApd Vgat$^+$ neurons likely eventually converge onto the mesolimbic circuit to mediate social reward behavior.

We show that the effect of MeApd neurons on social reward and reinforcement could be mediated by the MPOA-projecting MeApd circuitry. The MPOA is a highly heterogeneous brain structure that contains multiple partially overlapping subpopulations marked by the expression of *Nts*, *Esr1* and *Gal* genes, each of which consists of a mix of glutamatergic and GABAergic neurons[11,34,35]. Although these various MPOA populations project directly to the VTA, the synaptic mechanism of how these neurons promote dopamine release in the NAc is still largely unclear. Indeed, both glutamatergic and GABAergic populations send direct monosynaptic inputs to the VTA[34] and might exert opposite effects. Thus, understanding how MeApd Vgat$^+$ neurons promote dopamine release requires a full picture of the MPOA-VTA-NAc circuitry and remains an important topic for future investigation. Our findings provide new insights into the understanding of the circuitry that connects the amygdala and the hypothalamus and their roles in regulating social behavior and reinforcement. As drugs of abuse lead to addiction by taking control of normal brain reward circuits that reinforce essential behaviors[33,42], the MeApd-to-MPOA pathway could be a previously underappreciated target of drugs of abuse that deserves further studies.

Animals engage in specific types of social behavioral actions within immediate social contexts, such as aggressive behavior in males[16,43] or sexual attraction between males and females[11,26,44,45]. The motivation that drives these specific moment-by-moment actions tends to be highly context dependent and likely involves distinct neural circuits[11,16,26,43,44]. As the MeA was previously shown to play an important role in aggressive behavior in males and sexual responses in females, the role of MeApd Vgat$^+$ neurons in mediating general social reward toward juvenile animals in both males and females might reflect a distinct behavioral function. Indeed, a different subpopulation of the MeA (*Nos1*$^+$) promotes female animals' sexual responses toward male pheromones and can also drive reinforcement behavior[26]. These neurons are enriched in the posteroventral subdivision of the MeA (MeApv), which regulates sexual receptivity and mating behavior in females[23]. As the MeApd consists of heterogeneous subpopulations of GABAergic neurons[13,46], it remains to be determined whether distinct GABAergic subtypes might play distinct roles in social reward and/or other social behaviors and whether these diverse behavioral functions are mediated by the same or distinct neuronal subtypes.

Moreover, involvement of a brain area in processing social information does not necessitate its requirement for social reward and/or positive reinforcement. For example, although the ventromedial hypothalamus was shown to drive specific social behavior, it

Fig. 7 | Activation of the MeApd-to-MPOA circuit overcomes avoidance behavior. a,**b**, Schematic showing optogenetic stimulation in a modified open field test. Optogenetic stimulation is coupled with the center area (blue) and is triggered when animals enter this area. **c**,**f**, Schematic showing viral injection and fiber placement for ChR2 stimulation of Vgat$^+$ neuron cell bodies in the MeApd or their axonal terminals in the MPOA. **d**,**g**, Representative heat maps of locomotion trajectories of ChR2-expressing animals after stimulation. **e**,**h**, ChR2-expressing animals spent more time in the stimulation-coupled area (center) than control animals. **k**,**n**, Schematic showing optogenetic stimulation paradigm in a modified elevated plus maze test. **i**,**j**, Optogenetic stimulation is coupled with the two open arms (blue) and is triggered when animals enter this area. **k**,**n**, Schematic showing ChR2 stimulation of Vgat$^+$ neuron cell bodies in the MeApd or their axonal terminals in the MPOA. **l**,**o**, Representative heat maps of locomotion trajectories of ChR2-expressing animals after stimulation. **m**,**p**, ChR2-expressing animals spend more time in the stimulation-coupled open arms compared to controls. In **d** and **e**, $n=8$ mice (ChR2) and 6 mice (control); in **g** and **h**, $n=5$ mice (ChR2) and 5 mice (control); in **l** and **m**, $n=8$ mice (ChR2) and 17 mice (control); in **o** and **p**, $n=10$ mice (ChR2) and 5 mice (control). Two-way repeated-measures ANOVA with Bonferroni post hoc correction (*$P<0.05$, ** $P<0.01$, ***$P<0.001$). Data are shown as mean ± s.e.m. For detailed statistical information, see Supplementary Table 1.

does not appear to promote positive reinforcement[16]. Moreover, activation of MeApv Drd+ neuron projection to the bed nucleus of stria terminalis increases aggression, but it does not appear to promote positive reinforcement[17]. Lastly, activating neurons in the dorsomedial prefrontal cortex that are directly involved in social behavior does not lead to positive reinforcement[18]. These findings suggest that processing positive social signals and promoting positive reinforcement are not a non-specific feature of social brain areas but recruit specific circuits and neuronal populations. Thus, Vgat+ neurons in the MeApd do not simply relay social information but likely represent a specific node among social brain areas that is both necessary and sufficient to drive positive reinforcement. Indeed, Vglu2+ neurons in the MeApd do not promote positive reinforcement, further suggesting that the role of Vgat+ neurons in social

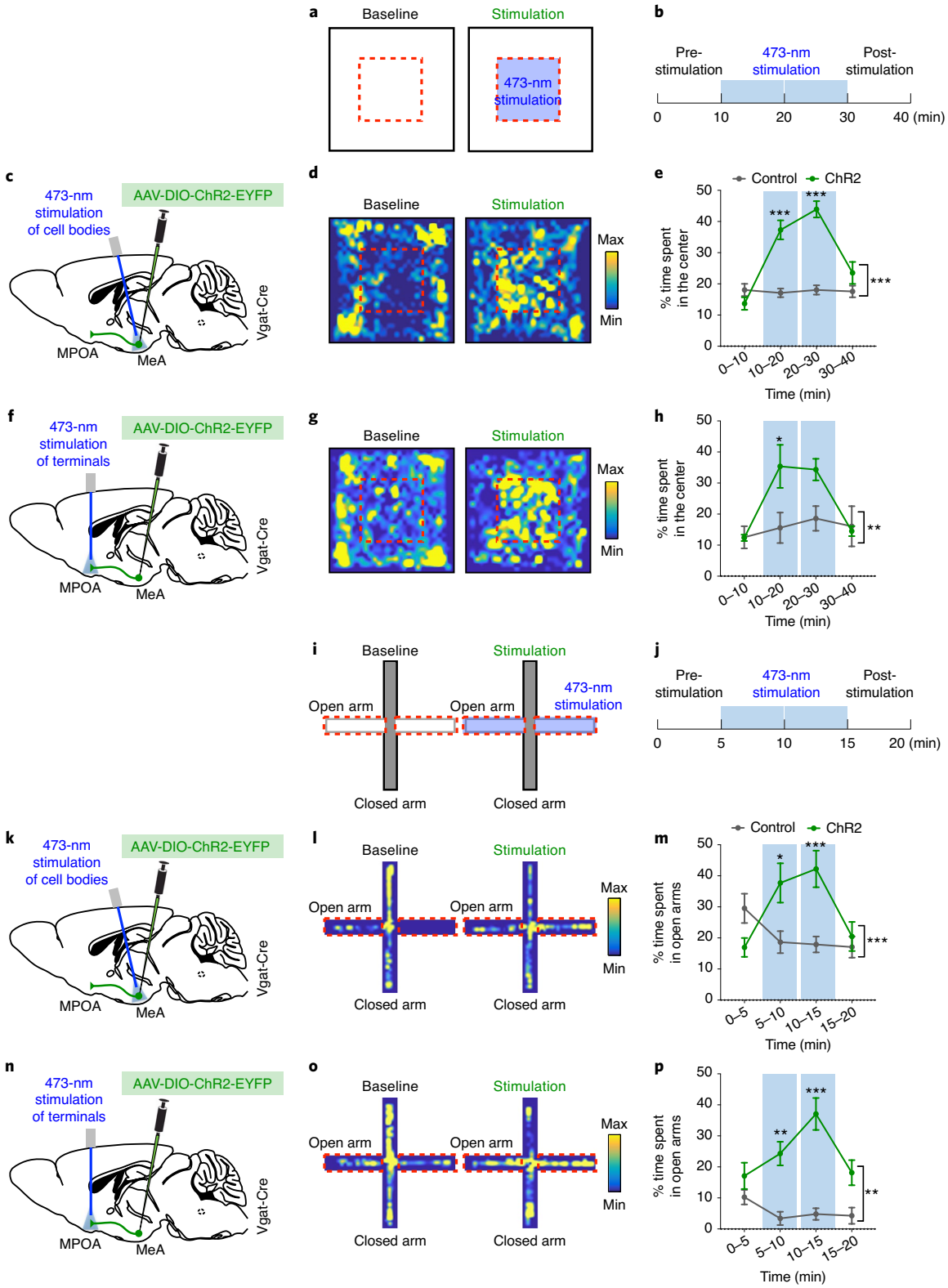

reward is specific and is functionally separable from Vglut2$^+$ neurons in the same brain area.

Finally, social impairment is a core symptom of many neurodevelopmental and neuropsychiatric disorders, such as autism spectrum disorders, depression and anxiety[6,7,47]. As positive social experiences play a critical role in buffering against aversive experiences, impairment of social functions and resulting lack of social experiences might lead to a wide variety of health problems[2,36,48]. How social processing overcomes negative experiences, and the neural mechanisms underlying these functions, have been largely unclear. We showed that the rewarding effect produced by the activation of the MeApd circuit is sufficient to overcome behavior associated with negative experiences. This suggests that a potential mechanism of counterbalancing negative experiences is through the activation of circuits that directly regulate social reward.

Online content

Any methods, additional references, Nature Research reporting summaries, source data, extended data, supplementary information, acknowledgements, peer review information; details of author contributions and competing interests; and statements of data and code availability are available at https://doi.org/10.1038/s41593-021-00828-2.

Received: 21 July 2020; Accepted: 26 February 2021;
Published online: 5 April 2021

References

1. Stanley, D. A. & Adolphs, R. Toward a neural basis for social behavior. *Neuron* **80**, 816–826 (2013).
2. Umberson, D., Crosnoe, R. & Reczek, C. Social relationships and health behavior across the life course. *Annu. Rev. Socio.* **36**, 139–157 (2010).
3. Chen, P. & Hong, W. Neural circuit mechanisms of social behavior. *Neuron* **98**, 16–30 (2018).
4. Tamir, D. I. & Hughes, B. L. Social rewards: from basic social building blocks to complex social behavior. *Perspect. Psychol. Sci.* **13**, 700–717 (2018).
5. Hu, H. Reward and aversion. *Annu. Rev. Neurosci.* **39**, 297–324 (2016).
6. Chevallier, C., Kohls, G., Troiani, V., Brodkin, E. S. & Schultz, R. T. The social motivation theory of autism. *Trends Cogn. Sci.* **16**, 231–239 (2012).
7. Zeeland, A. A. S.-V., Dapretto, M., Ghahremani, D. G., Poldrack, R. A. & Bookheimer, S. Y. Reward processing in autism. *Autism Res.* **3**, 53–67 (2010).
8. Nieh, E. H. et al. Inhibitory input from the lateral hypothalamus to the ventral tegmental area disinhibits dopamine neurons and promotes behavioral activation. *Neuron* **90**, 1286–1298 (2016).
9. Hung, L. W. et al. Gating of social reward by oxytocin in the ventral tegmental area. *Science* **357**, 1406–1411 (2017).
10. Dölen, G., Darvishzadeh, A., Huang, K. W. & Malenka, R. C. Social reward requires coordinated activity of nucleus accumbens oxytocin and serotonin. *Nature* **501**, 179 (2013).
11. McHenry, J. A. et al. Hormonal gain control of a medial preoptic area social reward circuit. *Nat. Neurosci.* **20**, 449–458 (2017).
12. Hong, W., Kim, D.-W. & Anderson, D. J. Antagonistic control of social versus repetitive self-grooming behaviors by separable amygdala neuronal subsets. *Cell* **158**, 1348–1361 (2014).
13. Chen, P. B. et al. Sexually dimorphic control of parenting behavior by the medial amygdala. *Cell* **176**, 1206–1221 (2019).
14. Lin, D. et al. Functional identification of an aggression locus in the mouse hypothalamus. *Nature* **470**, 221–226 (2011).
15. Wu, Z., Autry, A. E., Bergan, J. F., Watabe-Uchida, M. & Dulac, C. G. Galanin neurons in the medial preoptic area govern parental behaviour. *Nature* **509**, 325 (2014).
16. Falkner, A. L., Grosenick, L., Davidson, T. J., Deisseroth, K. & Lin, D. Hypothalamic control of male aggression-seeking behavior. *Nat. Neurosci.* **19**, 596–604 (2016).
17. Miller, S. M., Marcotulli, D., Shen, A. & Zweifel, L. S. Divergent medial amygdala projections regulate approach-avoidance conflict behavior. *Nat. Neurosci.* **22**, 565–575 (2019).
18. Gutzeit, V. A. et al. Optogenetic reactivation of prefrontal social neural ensembles mimics social buffering of fear. *Neuropsychopharmacology* **45**, 1068–1077 (2020).
19. Swanson, L. W. Cerebral hemisphere regulation of motivated behavior. *Brain Res.* **886**, 113–164 (2000).
20. Choi, G. B. et al. Lhx6 delineates a pathway mediating innate reproductive behaviors from the amygdala to the hypothalamus. *Neuron* **46**, 647–660 (2005).
21. Li, Y. et al. Neuronal representation of social information in the medial amygdala of awake behaving mice. *Cell* **171**, 1176–1190 (2017).
22. Bergan, J. F., Ben-Shaul, Y. & Dulac, C. Sex-specific processing of social cues in the medial amygdala. *eLife* **3**, e02743 (2014).
23. Ishii, K. K. et al. A labeled-line neural circuit for pheromone-mediated sexual behaviors in mice. *Neuron* **95**, 123–137 (2017).
24. Unger, E. K. et al. Medial amygdalar aromatase neurons regulate aggression in both sexes. *Cell Rep.* **10**, 453–462 (2015).
25. Yao, S., Bergan, J., Lanjuin, A. & Dulac, C. Oxytocin signaling in the medial amygdala is required for sex discrimination of social cues. *eLife* **6**, e31373 (2017).
26. Demir, E. et al. The pheromone darcin drives a circuit for innate and reinforced behaviours. *Nature* **578**, 137–141 (2020).
27. Golden, S. A. et al. Compulsive addiction-like aggressive behavior in mice. *Biol. Psychiatry* **82**, 239–248 (2017).
28. Venniro, M. et al. Volitional social interaction prevents drug addiction in rat models. *Nat. Neurosci.* **21**, 1520–1529 (2018).
29. Martin, L. & Iceberg, E. Quantifying social motivation in mice using operant conditioning. *J. Vis. Exp.* e53009 (2015).
30. Jacobs, S., Huang, F., Tsien, J. & Wei, W. Social recognition memory test in rodents. *Bio-protocol* **6**, e1804 (2016).
31. Hlinák, Z. & Krejcí, I. Social recognition in male rats: age differences and modulation by MIF-I and Alaptide. *Physiol. Res.* **40**, 59–67 (1991).
32. Berke, J. D. What does dopamine mean? *Nat. Neurosci.* **21**, 787–793 (2018).
33. Volkow, N. D., Wise, R. A. & Baler, R. The dopamine motive system: implications for drug and food addiction. *Nat. Rev. Neurosci.* **18**, 741–752 (2017).
34. Fang, Y.-Y., Yamaguchi, T., Song, S. C., Tritsch, N. X. & Lin, D. A hypothalamic midbrain pathway essential for driving maternal behaviors. *Neuron* **98**, 192–207.e10 (2018).
35. Kohl, J. et al. Functional circuit architecture underlying parental behaviour. *Nature* **556**, 326–331 (2018).
36. Hennessy, M. B., Kaiser, S. & Sachser, N. Social buffering of the stress response: diversity, mechanisms, and functions. *Front. Neuroendocrinol.* **30**, 470–482 (2009).
37. Nardou, R. et al. Oxytocin-dependent reopening of a social reward learning critical period with MDMA. *Nature* **569**, 116–120 (2019).
38. Schultz, W. Dopamine reward prediction-error signalling: a two-component response. *Nat. Rev. Neurosci.* **17**, 183–195 (2016).
39. Collins, A. L. et al. Dynamic mesolimbic dopamine signaling during action sequence learning and expectation violation. *Sci. Rep.* **6**, 20231 (2016).
40. Prévost-Solié, C., Girard, B., Righetti, B., Tapparel, M. & Bellone, C. Dopamine neurons of the VTA encode active conspecific interaction and promote social learning through social reward prediction error. Prerint at *bioRxiv* https://doi.org/10.1101/2020.05.27.118851 (2020).
41. Padilla, S. L. et al. Agouti-related peptide neural circuits mediate adaptive behaviors in the starved state. *Nat. Neurosci.* **19**, 734–741 (2016).
42. Berke, J. D. & Hyman, S. E. Addiction, dopamine, and the molecular mechanisms of memory. *Neuron* **25**, 515–532 (2000).
43. Golden, S. A. et al. Basal forebrain projections to the lateral habenula modulate aggression reward. *Nature* **534**, 688 (2016).
44. Beny-Shefer, Y. et al. Nucleus accumbens dopamine signaling regulates sexual preference for females in male mice. *Cell Rep.* **21**, 3079–3088 (2017).
45. Kingsbury, L. et al. Cortical representations of conspecific sex shape social behavior. *Neuron* **107**, 941–953 (2020).
46. Wu, Y. E., Pan, L., Zuo, Y., Li, X. & Hong, W. Detecting activated cell populations using single-cell RNA-seq. *Neuron* **96**, 313–329 (2017).
47. Kupferberg, A., Bicks, L. & Hasler, G. Social functioning in major depressive disorder. *Neurosci. Biobehav. Rev.* **69**, 313–332 (2016).
48. Matthews, G. A. et al. Dorsal raphe dopamine neurons represent the experience of social isolation. *Cell* **164**, 617–631 (2016).

Methods

Animals. C57BL/6J males and females (8–12 weeks old) were purchased from Jackson Laboratory and used for behavioral experiments. Slc32a1-ires-Cre (Vgat-Cre) and Slc17a6-ires-Cre (Vglut2-Cre) mice[49] were purchased from Jackson Laboratory (stock nos. 028862 and 028863) and were crossed to C57BL/6J mice (purchased from Jackson Laboratory) to produce heterozygous animals ($Vgat^{Cre/+}$ and $Vglut2^{Cre/+}$, 8–16 weeks old, both males and females) for stereotaxic surgery and behavioral experiments. Juvenile animals (4–6 weeks old) used as social stimuli in the social operant task were produced from our breeding colony. Animals were housed on a 12-h light/dark cycle (22:00–10:00 light) with food and water available ad libitum. Care and experimental manipulations of all animals were carried out in accordance with the National Institutes of Health Guide for Care and Use of Laboratory Animals and approved by the Institutional Animal Care and Use Committee at the University of California, Los Angeles.

Viruses. AAV2-Syn-EYFP, AAV2-EF1α-DIO-EYFP, AAV2-EF1α-FLEX-mCherry, AAV2-EF1α-DIO-hChR2-EYFP and AAV2-DIO-taCasp3-TEVp[50] were purchased from the University of North Carolina Viral Vector Core. AAV1-hSyn1-SIO-stGtACR2-FusionRed[51] (cat. no. 105677-AAV1), AAV1-syn-FLEX-jGCaMP7f-WPRE[52] (cat. no. 104492-AAV1), AAV5-hSynapsin1-FLEX-axon-GCaMP6s[53] (cat. no. 112010-AAV5), AAV1-mDlx-NLS-mRuby2 (ref. [54]) (cat. no. 99130-AAV1), AAVretro-hSyn-HI-eGFP-Cre (cat. no. 105540-AAVrg) and AAV5-hSyn-dLight1.2 (ref. [55]) (cat. no. 111068-AAV5) were purchased from Addgene. CTB-Alexa Fluor 647 was purchased from Thermo Fisher Scientific (cat. no. C34778).

Stereotaxic surgeries. $Vgat^{Cre/+}$ and $Vglut2^{Cre/+}$ animals (8–16 weeks old) were anesthetized with isoflurane and mounted on a stereotaxic device (Kopf Instruments). Both males (>20 g) and females (>16 g) were used in the experiments. Injections were carried out using a pulled, fine glass capillary (WPI).

For caspase-mediated ablation of MeApd $Vgat^+$ neurons, Vgat-Cre mice were injected bilaterally with 350 nl of AAV2-DIO-taCasp3-TEVp and 50 nl of AAV2-EF1α-DIO-hChR2-EYFP into the MeApd (ML ±2.05, AP −1.5~−1.6, DV −5.25 from bregma).

For caspase-mediated ablation of MPOA-projecting MeApd neurons, C57BL/6J mice were bilaterally injected with 300 nl of AAV-retro-eGFP-Cre into the MPOA (ML ±0.4, AP −0.1, DV −5.0 from bregma) and 400 nl of AAV2-DIO-taCasp3-TEVp into the MeApd (ML ±2.05, AP −1.5~−1.7, DV −5.25 from bregma).

For optogenetic activation or silencing of MeApd neuron cell bodies, Vgat-Cre mice were injected bilaterally with 400 nl of AAV1-hSyn1-SIO-stGtACR2-FusionRed into the MeApd for inhibition or 200–250 nl of AAV2-EF1α-DIO-hChR2-EYFP into the MeApd for activation (MeApd: ML ±2.05, AP −1.5~−1.7, DV −5.25 from bregma). An optic fiber (200-μm core diameter, Inper) was then placed 0.4–0.5 mm above the virus injection site in the MeApd.

For fiber photometry recording of calcium signals, Vgat-Cre mice were injected with 200 nl of AAV1-syn-FLEX-jGCaMP7f-WPRE or AAV5-hSynapsin1-FLEX-axon-GCaMP6s into the MeApd (ML ±2.05, AP −1.5~−1.6, DV −5.15~−5.25 from bregma). An optic fiber (200-μm core diameter, Inper) was implanted 0.2 mm above the injection site in the MeApd or at its downstream projection target in the MPOA (ML ±0.4, AP −0.1, DV −5.0 from bregma).

For fiber photometry recording of dopamine signals in the NAc during the social operant task, C57BL/6J mice were injected with 200−250 nl of AAV5-hSyn-dLight1.2 (or AAV2-Syn-EYFP as a control) into the NAc (ML 1.20, AP +1.20, DV −4.30 from bregma). An optic fiber (200-μm core diameter, Inper) was implanted at the virus injection site in the NAc.

For fiber photometry recording of dopamine signals in the NAc in response to activation of MeApd $Vgat^+$ neurons, Vgat-Cre mice were injected with 300 nl of AAV5-hSyn-dLight1.2 into the NAc (ML 1.20, AP +1.20, DV −4.30 from bregma) and 200−250 nl of AAV2-EF1α-DIO-hChR2-EYFP into the MeApd (ML ±2.05, AP −1.5~−1.6, DV −5.25 from bregma). Two optic fibers (200-μm core diameter, Inper) were then implanted, one at the injection site in the NAc and the other 0.5 mm above the injection site in the MeApd.

For optogenetic activation of MeApd projections, Vgat-Cre mice were injected bilaterally (ML ±2.05, AP −1.5~−1.7, DV −5.25 from bregma) with 250 nl of AAV2-EF1α-DIO-hChR2-EYFP into the MeApd. Optic fibers were then implanted 0.4–0.5 mm above the MPOA (left side: ML −0.4, AP −0.1, DV −4.75 from bregma; right side, angled 6°, ML 1.0, AP −0.1, DV −4.8 from bregma) or above the PMV (left side: ML −0.5, AP −2.3, DV −5.10 from bregma; right side, ML 1.0, AP −2.3, DV −5.15 from bregma with a 3° angle). To rule out the possibility that stimulation of axonal terminals in the MPOA might lead to backpropagation of action potentials to cell bodies in the MeApd and other collateral projections, lidocaine (10 μg per 0.3 μl) was locally infused through a guide cannula into the MeApd.

For optogenetic inhibition of the MeApd-to-MPOA circuit, C57BL/6J mice were bilaterally injected with 300 nl of AAV-retro-eGFP-Cre into the MPOA (ML ±0.4, AP −0.1, DV −5.0 from bregma) and 400 nl of AAV1-hSyn1-SIO-stGtACR2-FusionRed (ML ±2.05, AP −1.5~−1.7, DV −5.25 from bregma) and then bilaterally implanted with optic fibers above the MeApd (ML ±2.05, AP −1.5~−1.7, DV −4.75 from bregma).

For characterization of MeApd GABAergic and glutamatergic neurons that project to the MPOA, Vglut2-Cre mice were injected with 300 nl of AAV-DIO-EYFP and 100 nl of AAV-mDlx-NLS-mRuby2 into the MeApd (ML ±2.05, AP −1.5~−1.7, DV −5.25 from bregma). Ten days after the initial injection, 200 nl of CTB-Alexa Fluor 647 was injected into the MPOA (ML ±0.4, AP −0.1, DV −5.0 from bregma) of the same animal. Dlx has been previously shown to specifically label GABAergic neurons[56]. We confirm that the expression of Dlx and Vglut2 promotors shows little overlap in the MeApd (Extended Data Fig. 10d).

All control animals in this study were animals with the same genetic background injected with EYFP-expressing or mCherry-expressing AAVs.

Behavioral assays. *Automated social operant task for quantitative analysis of social reward.* Based on previous work[16,27–29], we developed a fully automated, closed-loop operant conditioning system to quantitatively and efficiently measure social reward. The system consists of two chambers (Fig. 1a,b): a smaller one for holding the target animal and a larger one for placing the subject animal. The two chambers are separated by a metal wire grid (5 cm × 9 cm) that prevents animals from going to each other's chambers but allows the subject animal to sniff and investigate the target animal. Behind the wire gird is an opaque plastic door that can be automatically opened or closed by a motor, which is directly controlled by an Arduino microcontroller with custom code. Two 13-mm-diameter nose-poke ports (that is, social and non-social (null) ports) are located on two sides of the gate. Nose-pokes are detected by infrared beam sensors connected to the Arduino microcontroller. Nose-poking the social port initiates a new 10-s trial, which consists of a 3-s delay period and a 7-s social interaction period during which the gate is opened. The gate starts to open at 3 s, becomes fully opened at 5 s, starts to close at 8 s and becomes fully closed at 10 s (gate opening and closure takes 2 s to complete). Nose-poking the null port initiates a 10-s timeout period without gate opening and social interaction (Fig. 1b). Our social operant task consists of three phases, which include baseline (1 d), training (7 d) and post-training (2 d) (Fig. 1b). Compared to previous operant conditioning systems for social motivation, we also restricted the target animal in a smaller chamber (while the target animal can still move freely), increasing the chance of close social interaction when the gate opens.

In experiments presented in Fig. 1, wild-type mice were housed in our animal colony for at least 1 week. Before experiments, mice were habituated in the behavioral rig for 30 min with the ports blocked for 1–2 d. After habituation, on day 0 (baseline phase) we tested the baseline preference for the ports by allowing the mouse to freely poke the ports without door opening for 30 min. To counterbalance individual bias toward a specific port that is unrelated to social preference, the port with fewer nose-pokes for each animal was designated as the social port and the other port as the non-social (null) port for subsequent experiments. On days 1–7 (training phase), each mouse was trained in a 30-min daily session with door opening and social presentation (Fig. 1c,f). An unfamiliar male juvenile animal was used, and a different juvenile mouse was used each day over the 7-d training sessions. Although poking the null port does not lead to gate opening or social stimulus, it does lead to a 10-s timeout, which serves as a competing choice that animals have to select for or against during the training process. On days 8–9 (post-training phase), each mouse was trained in a 30-min daily session without target animals during the 'interaction' phase. To rule out the possibility that the preference for the social port was solely caused by gate opening, we also carried out control experiments in which mice were trained with gate opening in the absence of target animals when poking the social port.

Preference for the social port was calculated as the differences between the percentage of trials with nose-poking in the social port and the percentage of trials with nose-poking in the null port. To provide a descriptive characterization of animals exhibiting persistent social reward behavior, we chose a threshold for consistent preference (defined as showing greater than 20% preference for the social port on both day 6 and day 7) (Extended Data Fig. 1). However, statistical analysis was done with the full distribution of preferences from all animals without using any cutoff. Behaviors were recorded and quantified on days 1 and 7. We measured the anticipatory waiting time before gate opening, percentage of trials showing anticipatory behavior, latency to social interaction or exploration of the open gate, duration of interaction or exploration and percentage of trials with interaction. Period of social interaction was defined as the moment when subject animals stood in front of the gate and sniffed the target animal behind the gate. After poking the null port, animals sometimes incorrectly display anticipatory behavior (waiting in front of the gate during the delay period; Fig. 1m,n) as well as staying in front of the gate attempting to interact with animals behind the gate (Fig. 1o,p).

$Vgat^{Cre/+}$ mice produced in our breeding colony tend to show an overall lower number of nose-pokes (in both social and null ports) compared to wild-type C57BL/6J animals purchased from Jackson Laboratory, suggesting that the general motivation to engage in nose-poking could be different in animals with different transgenetic backgrounds and/or housing conditions. In all experiments, we did not proceed with training if animals exhibited no or little motivation to engage in nose-poke on both of the first 2 d of training (defined as fewer than ten total pokes in both social and null ports on each day).

To examine behavior that subject animals displayed toward juvenile animals during free social interactions before being trained in the social operant task, we

performed a free social interaction test (Extended Data Fig. 1a–c), in which the subject animal freely interacts with an unfamiliar male juvenile mouse for 10 min in a standard mouse cage. Social behaviors were annotated and quantified, which include sniffing (toward the body trunk, anogenital area or facial area), following, allogrooming, attacking and mounting.

Operant task for food reward. Animals were trained to press levers to obtain food reward (Extended Data Fig. 5) using an operant task chamber (Med Associates). The training procedure includes 3 d of magazine training and 3 d of operant training. Briefly, mice were initially food deprived for 18 h before the first training day. On days 1–3, animals were subject to daily magazine training sessions, in which each mouse received one food pellet (20 mg, Bio-Serv) per minute without lever pressing for 30 min. After each daily training session, subject animals were provided an excessive amount of food pellets before being food deprived for 14 h (20:00–10:00) before the next training session. On days 4–6, animals were subject to daily operant training sessions, in which each mouse was trained for 30 min to lever press to obtain food pellets. Pressing the lever paired with food reward led to the delivery of one food pellet after a brief delay (0.5 s on days 4 and 5 for association and 3 s on day 6 for testing), whereas pressing the other lever (the null lever) leads to a 10-s timeout.

Caspase-3 ablation experiments. In caspase-3-mediated ablation experiments, preferences for social reward were measured by the social operant task described above. Preferences for food-seeking behavior were measured by the operant task for food reward described above. Caspase-3-expressing and EYFP-expressing $Vgat^{Cre/+}$ mice were trained in the social operant task (Fig. 2a–h) or food operant task (Extended Data Fig. 5) ~3.5 weeks (for soma ablation) or ~5 weeks (for ablating MPOA-projecting MeA neurons) after viral injection. $Vgat^{Cre/+}$ mice (both caspase-3- and EYFP-expressing animals) showed an overall lower number of nose-pokes (in both social and null ports) compared to wild-type animals.

GtACR inhibition experiments. Optogenetic inhibition in social operant task. GtACR inhibition experiments (Figs. 2 and 6) were performed over three consecutive days after animals established a positive preference for the social port in the social operant task. Sham stimulation (no laser illumination) was performed on days 1 and 3, and optogenetic inhibition was performed on day 2. Each day consisted of 5 min of baseline and 5 min of sham or real stimulation (continuous 473-nm laser illumination). Before each experiment, a ferrule patch cord was coupled to the ferrule fiber implanted in the mouse using a zirconia split sleeve (Doric Lenses). An Arduino microcontroller board and a customized MATLAB program were used to control the initiation and termination of the test.

Free social interaction assay. A 3-min free social interaction session was performed daily on two consecutive days to examine various social behavior when subject animals freely interacted with a juvenile animal (Extended Data Fig. 3). Before each session, subject animals were habituated in a standard mouse cage for 3 min after being connected a ferrule patch cord. An unfamiliar juvenile male mouse was introduced into the cage for 3 min (different juveniles were used in different sessions). In one of two daily sessions (selected in a counterbalanced manner), continuous blue light stimulation was delivered to subject animals throughout the entire 3-min session. Social behaviors were annotated and quantified, which include sniffing (toward the body trunk, anogenital area or facial area), following, allogrooming, attacking and mounting. We compared the percent of time spent on different types of social behaviors between sham stimulation and blue light stimulation.

Three-chamber assay. Three-chamber assay was performed using a three-chamber apparatus that consists of two side compartments (25 cm × 25 cm) and a center compartment (12.5 cm × 25 cm) (illustrated in Extended Data Fig. 9e). In the first session, subject animals were introduced to the center compartment and allowed to freely explore all three compartments for 3 min. A stimulus mouse (4–6 weeks old) was then placed under an inverted wire cup in one side compartment (designated as social compartment), and an empty cup was placed in the other side compartment (designated as non-social compartment). Subject animals were allowed to explore all chambers for 3 min and tested daily on two consecutive days. In each daily session, one of the side compartments was selected as the social compartment in a counterbalanced manner on two consecutive days. One session is paired with optical stimulation and the other with no stimulation in a counterbalanced manner. The social preference was calculated as (time in social compartment − time in non-social compartment) / (time in social compartment + time in non-social compartment).

ChR2 activation experiments. ChR2 stimulations of MeApd neuron cell bodies or MeApd-to-MPOA circuit were performed using the following behavioral paradigms. Fiber attachment and laser control were done as in GtACR silencing experiments.

RTPP test. Mice were introduced into a two-chamber apparatus (60 cm × 30 cm × 30 cm for each chamber) and were allowed to freely move between the two chambers. Each test consisted of two consecutive 15-min sessions. In the first session, mice were allowed to freely explore the two compartments for 15 min, during which entering into one of the two chambers triggered optogenetic stimulation (ChR2: 473 nm, 20 ms and 20 Hz for soma stimulation or 473 nm, 5 ms and 50 Hz for terminal stimulation, 2.5 mW mm^{-2}, for up to 20-s duration). Exiting the stimulated chamber immediately terminated the photostimulation. During the second session, the opposite chamber was paired with photostimulation. An Arduino microcontroller board and a customized MATLAB program were used to control laser pulses, based on real-time tracking of mouse locations. Preference scores were calculated as the differences between percentages of time spent in the stimulated and unstimulated sides.

To examine the effect of potential backpropagation of action potentials to collateral branches, we performed a lidocaine infusion experiment during the RTPP test. On day 1 (ChR2 only), animals were subject to light stimulations in the RTPP test using procedures described above. On day 2 (ChR2 + lidocaine), a single dose of lidocaine (10 µg per 0.3 µl) was locally infused into the MeApd through an implanted guide cannula 10 min before the delivery of light stimulations in the RTPP test.

We also examined the effect of activating MeApd glutamatergic projections to the MPOA and MeApd GABAergic projections to the PMV in the RTPP test using procedures described above. Two daily sessions were performed on two consecutive days. Sham stimulation was performed on day 1 (baseline), and light stimulation was performed on day 2 (stimulation).

Intracranial self-stimulation. Mice were placed into a customized operant conditioning chamber (30 cm × 30 cm × 30 cm) that has two nose-poke ports (active and inactive) with infrared beam sensors. Nose-poking the active port triggered the delivery of photostimulation (ChR2: 473 nm, 20 ms and 20 Hz for soma stimulation or 473 nm, 5 ms and 50 Hz for terminal stimulation, 2.5 mW mm^{-2}, for up to 1-s duration), and withdrawal of the nose from the port terminated light stimulation. No stimulation was delivered when nose-poking the inactive port. The active and inactive ports were assigned randomly. Mice were allowed to freely explore the chamber for 10 min before the experiment for habituation to the experimental environment and were allowed to explore for 30 min during the experiment. An Arduino microcontroller board and a customized MATLAB program were used to control laser pulses.

Optogenetic reward task (mimicking social reward behavior). We modified the social operant task by replacing social interaction with 2-s light stimulation (ChR2: 473 nm, 20 ms and 20 Hz for soma stimulation or 473 nm, 5 ms and 50 Hz for terminal stimulation, 2.5 mW mm^{-2}) after the 3-s delay period. This test consisted of a 5-d training procedure (Figs. 3 and 6). On day 0 (baseline), we assessed the baseline preference for the ports by placing the mouse into the rig and letting it freely poke the ports without door opening for about 30 min. From day 1 to day 3 (training), each mouse was trained in a 30-min daily session with optical stimulation during the 'interaction' phase in the task (Figs. 3 and 6). On day 4 (post-training), each mouse was trained in a 30-min daily session without light delivery during the 'interaction' phase. Preference for the stimulation-coupled social port was calculated by subtracting the percentage of trials with nose-poking in the null port from the percentage of trials with nose-poking in the stimulated port. An Arduino microcontroller board and a customized MATLAB program were used to control laser pulses. We did not perform a social operant assay in which optogenetic stimulation is coupled with the presence of a target animal, as optogenetics stimulation alone is already sufficient to promote robust positive reinforcement and drive learning over days (Figs. 3 and 6).

Modified open field test. The open field test was done in a square chamber (50 × 50 × 50 cm). An experiment consisted of a 40-min test, which included four 10-min sessions of alternating laser stimulations (OFF–ON–ON–OFF). Mice were initially placed in the center of the chamber and allowed to freely explore the chamber. When the animals entered the center zone (25 × 25 cm), optical stimulation was delivered (ChR2: 473 nm, 20 ms and 20 Hz for soma stimulation or 473 nm, 5 ms and 50 Hz for terminal stimulation, 2.5 mW mm^{-2}, for up to 5-s duration). Exiting the center zone immediately terminated the photostimulation. Locations of animals (defined as position of the centroid) were tracked in real time using a customized program in MATLAB and were used to automatically control the Arduino microcontroller in a closed-loop manner.

Modified elevated plus maze. The elevated plus maze apparatus consisted of two open arms (30 cm × 5 cm) and two enclosed arms (30 cm × 5 cm × 30 cm) extending from a central intersection platform (5 cm × 5 cm). The apparatus was placed 75 cm from the floor. An experiment consisted of a 20-min test, which included four 5-min sessions of alternating laser stimulations (OFF–ON–ON–OFF). Mice were initially placed in the center of the chamber and allowed to freely explore the chamber. When animals entered the open arms, photostimulation was delivered (ChR2: 473 nm, 20 ms and 20 Hz for soma stimulation or 473 nm, 5 ms and 50 Hz for terminal stimulation, 2.5 mW mm^{-2}, for up to 10-s duration). Exiting the open arms immediately terminated the photostimulation. Locations of animals (defined as position of the centroid) were tracked in real time using a customized program in MATLAB and were used to automatically control the Arduino microcontroller in a closed-loop manner.

Electrophysiological recording in acute brain slices. Mice were anesthetized with isoflurane. The brain was rapidly dissected out and transferred to ice-cold oxygenated artificial cerebrospinal fluid (ACSF; 125 mM NaCl, 2.5 mM KCl, 2 mM $CaCl_2$, 1.3 mM NaH_2PO_4, 1.3 mM $MgCl_2$, 10 mM glucose and 25 mM $NaHCO_3$). Brain slices containing the MeApd were cut with a vibratome (300 µm; VT1200s, Leica). Brain slices were transferred to oxygenated ACSF and incubated at 33 °C for 1 h. All chemicals used in slice preparation were purchased from Sigma-Aldrich. Slices were then transferred to the recording chamber, which was submerged and perfused with ACSF at a rate of 3 ml min^{-1} at room temperature. Neurons were identified with differential interference contrast optics. The recording pipettes (3–5 MΩ) were prepared with a micropipette puller (P1000, Sutter Instrument). For cell-attached recordings, the pipettes were filled with an internal solution that contained the following (in mM): 130 K-gluconate, 10 HEPES, 0.6 EGTA, 5 KCl, 3 Na_2ATP, 0.3 Na_3GTP, 4 $MgCl_2$ and 10 Na_2-phosphocreatine (pH 7.2–7.4). The experiments were performed with a computer-controlled amplifier (MultiClamp 700B, National Instruments). The current and voltage signals were low-pass filtered at 3 kHz and digitized at 10 kHz (WinWCP software). Five-second continuous blue light (473 nm) was generated with a digitizer-controlled laser and delivered via an optic fiber cable onto the slice surface. The maximal light intensity reaching the brain tissue was ~10 mW. We analyzed the number of spikes before, during and after light stimulation.

Fiber photometry experiments and data analysis. Photometry experiments were performed as previously described[13]. Fluorescence signals were acquired with a fiber photometry system (Doric Lenses). The analog voltage signals were digitalized and recorded by a Micro 1401 digitizer (CED) and Spike2 software (v8.03). The LED power was adjusted at the tip of the optical fiber to 30–50 µW to minimize bleaching. Behaviors were recorded by a video camera (FLIR).

To record neuronal responses of MeApd Vgat$^+$ neurons and their projections to the MPOA during social interactions, subject animals were allowed to freely interact with a novel juvenile for ~20 s. To record neural responses in response to sucrose solution or chocolate, subject animals were allowed to freely consume sucrose solution or chocolate for ~5 min. Calcium signals were recorded during the presentation of social or non-social stimuli.

To record changes of dopamine signals in the NAc during social interactions (Fig. 4), we sequentially and pseudorandomly presented one male, female or juvenile mouse for ~10 s, with ~2-min inter-trial interval. We recorded dLight fluorescence at 100 Hz. Time 0 was defined as the moment when subject animals came in close contact with the target animal and began to investigate and sniff the target animal. Given the brief length (~10 s) of this initial investigation of stimulus animals (which is considered the appetitive phase of interaction), subject animals did not display aggressive or mating behavior, even toward adult conspecifics.

We also recorded dynamics of dopamine signals in the NAc in the social operant task. dLight-expressing animals were trained in the social operant task in the presence or absence of target animals. The behavior paradigm was similar to the procedures used and described in Fig. 1 with a few differences. Here, animals were trained for 7–12 daily sessions with target animals, and the well-trained status was defined as the day when animals reached stable social preference (20% social preference for at least three consecutive days). For animals trained in the presence of a target animal, dLight fluorescence was recorded on days 1 and 4 as well as the day when the animals reached the well-trained status (on days 7–12). On the day after training, an additional session of post-training test was recorded without target animals. For animals trained without target animals, dLight fluorescence was recorded on days 1, 4 and 7, as no animals reached well-trained status.

To record dopamine signals in the NAc during optical stimulation of MeApd Vgat$^+$ neurons, dLight signals in the NAc were recorded while delivering laser stimulation to the MeApd (473 nm, 20 Hz, 2.5 mW mm^{-2}, 20-ms pulses and 1-s stimulation duration), with ~ 1-min inter-trial interval. To prevent 473-nm laser stimulation delivered at the MeApd from contaminating fluorescence signals at the NAc, we recorded photometry signals at 1,000 Hz, filtered out data points that were acquired during any laser stimulation pulses (20 ms each at 20 Hz) and used only the data points that were temporally separate from any laser stimulation pulses for further analyses. This allowed us to effectively measure the true fluorescence signals from the NAc without any potential contamination of light signals coming from the laser stimulation at the MeApd.

Photometry data were analyzed using MATLAB. To measure the dynamics of fluorescence intensity immediately before and after the onset of specific behaviors or optogenetic stimulations, $(F-F_0)/F_0$ ($\Delta F/F$) was calculated, where F_0 was the baseline fluorescence signal averaged over a 1-s window between 5 s and 4 s (Fig. 4c–e and Extended Data Fig. 4), between 3 s and 2 s (Fig. 4h–k,m–o) or between 2 s and 1 s (Fig. 5b,c) before the behavior or stimulation onset. $\Delta F/F$ values were presented as mean with an s.e.m. envelope. To measure neural activity (that is, fluorescence changes of GCaMP) of MeApd Vgat$^+$ neurons in response to social and non-social stimuli (Extended Data Fig. 4), we calculated the area under the curve (AUC) per second between 0 s and 5 s from the behavior onset. To measure dopamine signals (that is, fluorescence changes of dLight) in the NAc during social interactions (Fig. 4a–e), we calculated the AUC per second between −1 s and 1 s relative to the behavior onset. To measure dopamine signals (that is, fluorescence changes of dLight) in the NAc during optogenetic stimulation of MeApd Vgat$^+$ neurons (Fig. 5b–e), we calculated the AUCs per second between 0 s and 1 s relative to the stimulation onset and between 0.3 s and 0.6 s after the termination of stimulation.

Histology and imaging. Animals were sacrificed 4–6 weeks after injection and perfused with 4% paraformaldehyde (PFA). The brains were dissected out and fixed in 4% PFA for two additional hours at room temperature, rinsed with 1× PBS and placed in 30% sucrose solution overnight at 4 °C. To visualize viral expression and fiber placement, 60-µm sections were cut on a Leica CM1950 cryostat. To examine dLight expression in the NAc, 60-µm sections were stained with chicken anti-GFP antibody (Aves Labs, no. 1020, 1:1,000) overnight at 4 °C and with donkey anti-chicken Alexa 488 antibody (Jackson ImmunoResearch, no. 703-545-155, 1:1,000) overnight at 4 °C. Images were acquired using a confocal microscope (Zeiss LSM 880).

Data analysis and statistics. No statistical methods were used to predetermine sample sizes, but our sample sizes were selected based on previous experience from related research and literature[12,13]. Animals were randomly assigned to control and manipulation groups. Data collection and analysis were not performed blinded to the conditions of experiments. Animals that exhibited no or little motivation to engage in nose-pokes on the first 2 d of training (defined as fewer than ten total pokes of the social and null ports on both days) were excluded from training and data collection. One EYFP-expressing animal in the photometry experiment was excluded based on this criterion. Animals that had low body weight (males <20 g and females <16 g) were excluded from surgeries and experiments. Behavior was analyzed using MATLAB code (https://pdollar.github.io/toolbox/). Figures were plotted using Prism version 9 (GraphPad) or MATLAB 2018b (MathWorks). Data are reported as box plots, dot plots or mean ± s.e.m. plots. In box plots, the central mark indicates the median; the bottom and top edges of the box indicate the 25th and 75th percentiles; and the whiskers indicate the 10th and 90th percentiles. Statistical methods used in this study include two-way repeated-measures analysis of variance (ANOVA), one-way repeated-measures ANOVA, one-way ANOVA, Kruskal–Wallis test (one-way ANOVA on ranks), two-sided Mann–Whitney test, two-sided unpaired *t*-test and two-sided paired *t*-test (Supplementary Table 1). The data met the assumptions of the statistical tests used. Normality of the data was tested using the Kolmogorov–Smirnov test. Statistically significant differences were established at $^*P<0.05$, $^{**}P<0.01$ and $^{***}P<0.001$; NS indicates not significant. All statistical tests are summarized in Supplementary Table 1.

Reporting Summary. Further information on research design is available in the Nature Research Reporting Summary linked to this article.

Data availability

All data generated and analyzed during this study are either included in this published article or available from the corresponding author upon reasonable request.

Code availability

Behavior was analyzed using MATLAB code, available at https://pdollar.github.io/toolbox/. The code that supports these findings is available upon reasonable request from the corresponding author.

References

49. Vong, L. et al. Leptin action on GABAergic neurons prevents obesity and reduces inhibitory tone to POMC neurons. *Neuron* **71**, 142–154 (2011).
50. Yang, C. F. et al. Sexually dimorphic neurons in the ventromedial hypothalamus govern mating in both sexes and aggression in males. *Cell* **153**, 896–909 (2013).
51. Mahn, M. et al. High-efficiency optogenetic silencing with soma-targeted anion-conducting channelrhodopsins. *Nat. Commun.* **9**, 4125 (2018).
52. Dana, H. et al. High-performance calcium sensors for imaging activity in neuronal populations and microcompartments. *Nat. Methods* **16**, 649–657 (2019).
53. Broussard, G. J. et al. In vivo measurement of afferent activity with axon-specific calcium imaging. *Nat. Neurosci.* **21**, 1272–1280 (2018).
54. Chan, K. Y. et al. Engineered AAVs for efficient noninvasive gene delivery to the central and peripheral nervous systems. *Nat. Neurosci.* **20**, 1172–1179 (2017).
55. Patriarchi, T. et al. Ultrafast neuronal imaging of dopamine dynamics with designed genetically encoded sensors. *Science* **360**, eaat4422 (2018).
56. Dimidschstein, J. et al. A viral strategy for targeting and manipulating interneurons across vertebrate species. *Nat. Neurosci.* **19**, 1743–1749 (2016).

Acknowledgements

We thank K. Wassum, P. Golshani, L. Kingsbury, T. Raam, D. Wei, L. Gu, F. Sun and M. Zhang for critical comments on this manuscript and P. Chen, S. Hu, H. Li, Y. Wu and P.

Zhao for technical assistance. This work was supported, in part, by NIH R01 NS113124, a Searle Scholars Award, a Klingenstein-Simons fellowship, a Brain Research Foundation grant, a Packard Foundation fellowship, a McKnight Scholar Award, a Keck Foundation Award, a Vallee Scholars Award and a Mallinckrodt Scholar Award to W.H. and a Marion Bowen postdoctoral grant to R.K.H.

Author contributions

R.K.H. and W.H. conceptualized and designed the study. R.K.H., Y.Z., T.L. and J.W. performed optogenetics and behavioral experiments. R.K.H. and T.L. performed fiber photometry and histology. R.K.H. analyzed behavioral and neural data. R.K.H. performed ex vivo electrophysiology experiments. P.M. provided suggestions on electrophysiology. R.K.H., Y.E.W. and W.H. wrote the manuscript. W.H. supervised the entire study, provided resources and acquired funding.

Competing interests

The authors declare no competing financial interests.

Additional information

Extended data is available for this paper at https://doi.org/10.1038/s41593-021-00828-2.

Supplementary information The online version contains supplementary material available at https://doi.org/10.1038/s41593-021-00828-2.

Correspondence and requests for materials should be addressed to W.H.

Peer review information *Nature Neuroscience* thanks Sam Golden, Olga Penagarikano and the other, anonymous, reviewer(s) for their contribution to the peer review of this work.

Reprints and permissions information is available at www.nature.com/reprints.

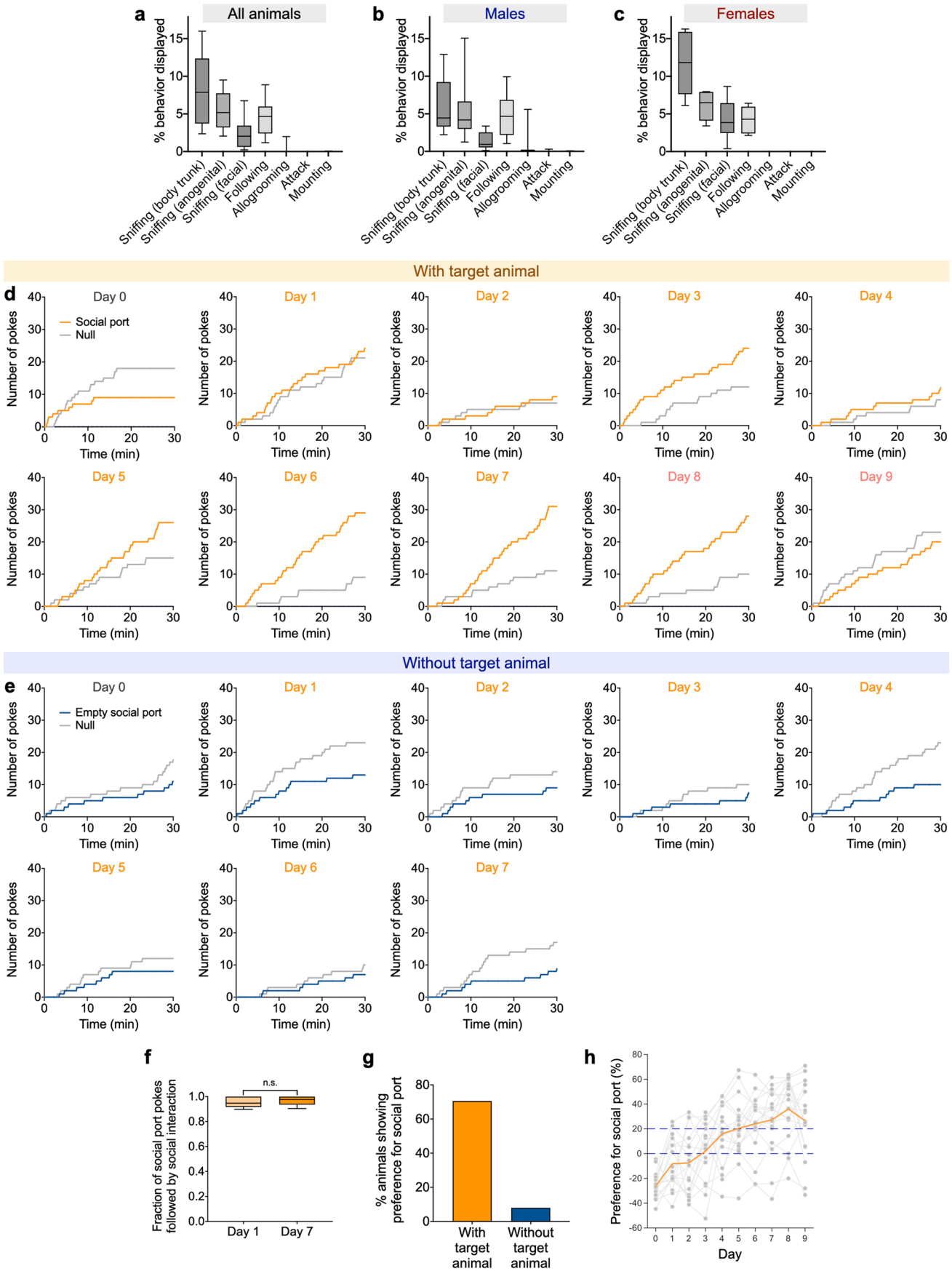

Extended Data Fig. 1 | See next page for caption.

Extended Data Fig. 1 | Characterizations of behaviors in free social interaction and social operant task. a-c, Fraction of time spent on seven distinct social behaviors displayed by adult animals (**a**, all animals; **b**, males; **c**, females) towards juvenile animals during free social interaction. Both male and female adult animals predominantly display close social investigation (sniffing) towards juvenile animals. The behavioral characterizations of these male and female animals in the social operant task are included in Extended Data Fig. 2. **d**, **e**, Cumulative distribution of the numbers of nose pokes in social and null ports in social operant task in one representative animal on each day. The assay was performed in the presence (**d**) or absence (**e**) of the target animal. **f**, The majority of social port pokes are followed by close social interaction between subject and target animals (across the barrier). $P = 0.2149$, Paired t test (two-sided). **g**, Percentage of animals showing consistent preference for the social port (defined as showing >20% preference on both days 6 and 7) in the presence or absence of the target animal. **h**, Full distribution of nose poke preferences in individual animals in Fig. 1i. Grey lines and dots indicate preferences of individual mice and orange line indicates the average across all animals. In (**a**-**c**), n = 12 males and 8 females; in (**f**), n = 17 mice; (**g**), n = 17 mice (with target animals) and 25 mice (without target animals); in (**h**), n = 17 mice. (**a**-**c**, **f**), boxplots: center = median, box = quartiles, whisker = 10 – 90 percentile. For detailed statistics information, see Supplementary Table 1.

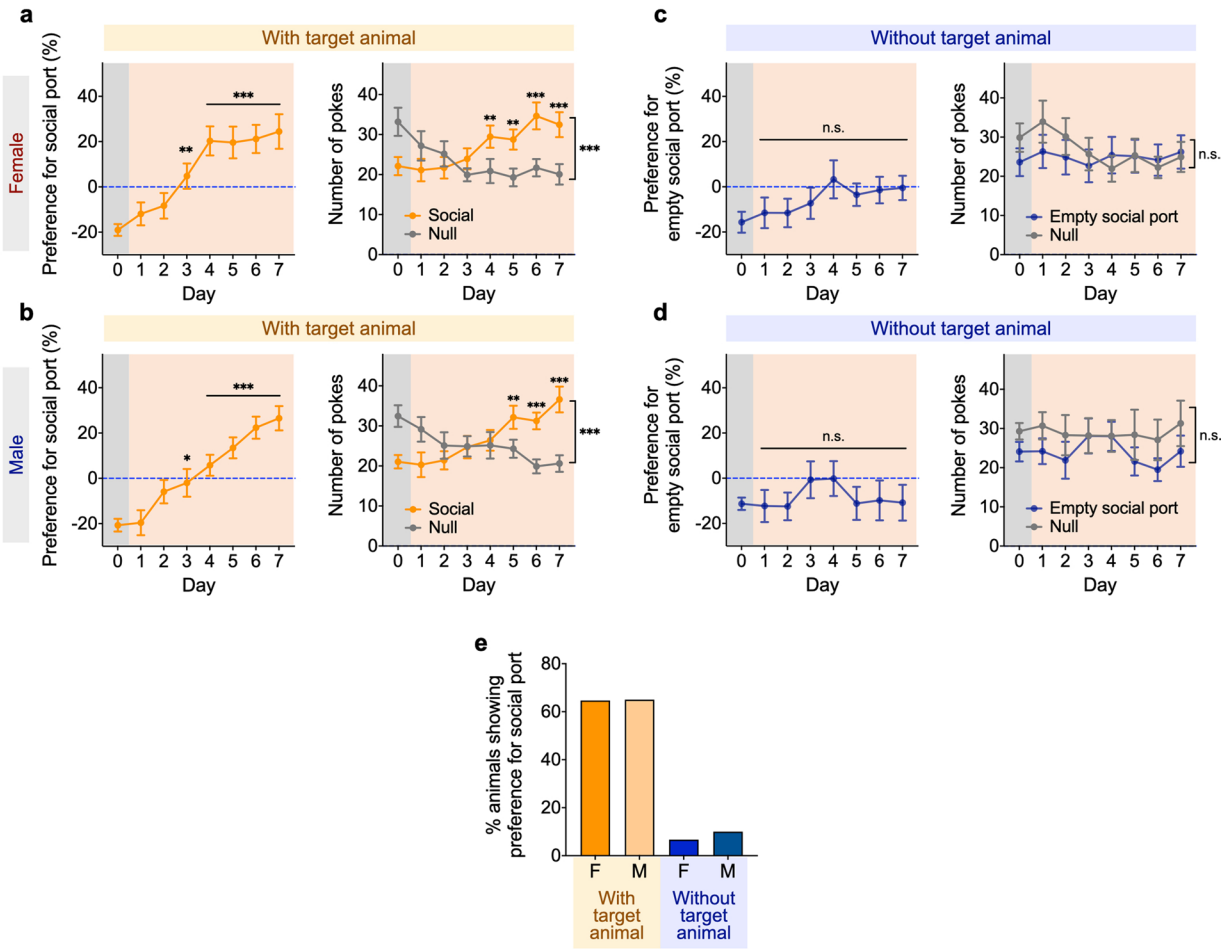

Extended Data Fig. 2 | Both male and female adult mice exhibit social reward behavior. a, b, Preference for social port and numbers of pokes in females (**a**) and males (**b**) in the presence of a target animal. Both male and female animals develop strong preference for the social port in the presence of target animals. Experiment was performed over a 10-day period, which consists of 1 day of baseline session, 7 days of training sessions with target animals, and 2 days of post-training sessions. **c, d**, Preference for social port and numbers of pokes in females (**c**) and males (**d**) in the absence of a target animal. Neither male nor female animals develop preference for the social port. Experiment was performed over an 8-day period, which consists of 1 day of baseline session and 7 days of training sessions without target animals. **e**, Percentage of male and female mice exhibiting consistent preference for social port (defined as showing >20% preference on both days 6 and 7). In (**a**, **b**, **e**), with target animals, n = 17 females and 20 males; these include 9 females and 8 males presented in Fig. 1 as well as an additional 8 females and 12 males presented in Extended Data Fig. 1. In (**c**, **d**, **e**), without target animals, n = 15 females and 10 males. In (**a**-**d**), left panels, one-way repeated measures ANOVA with Bonferroni post-hoc correction ($^{*}P < 0.05$, $^{**}P < 0.01$, $^{***}P < 0.001$); right panels, two-way repeated measures ANOVA with Bonferroni post-hoc correction ($^{**}P < 0.01$, $^{***}P < 0.001$). (**a**-**d**), mean ± SEM. For detailed statistics information, see Supplementary Table 1.

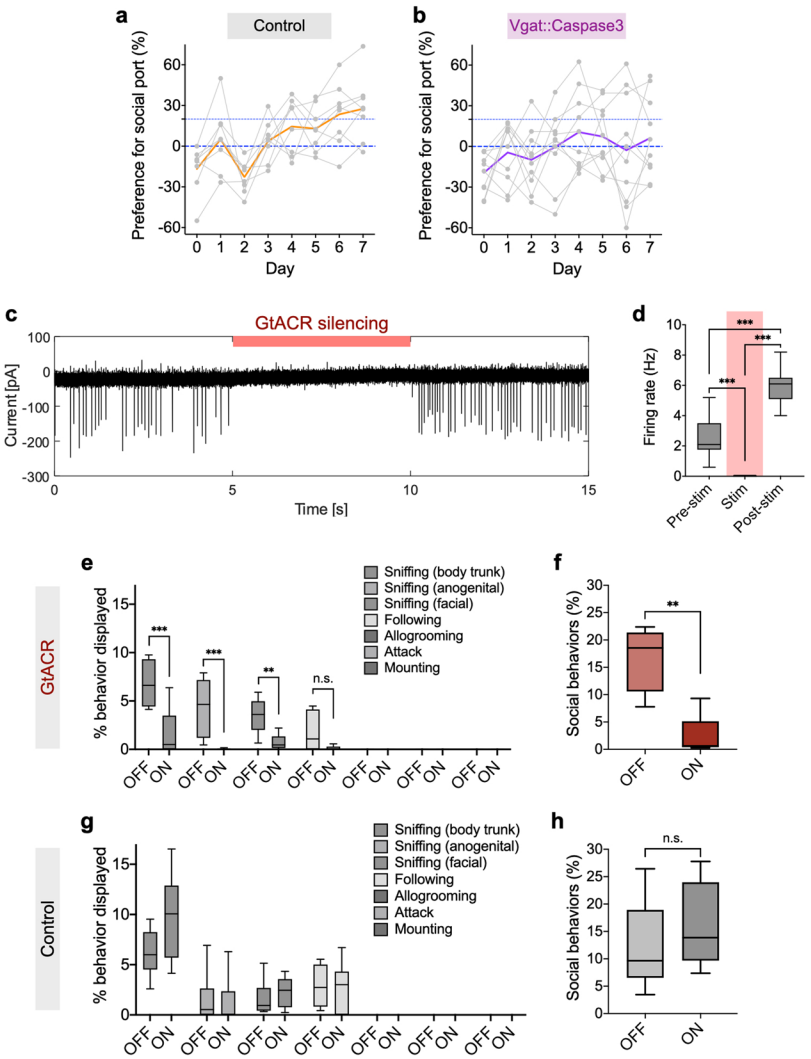

Extended Data Fig. 3 | Additional characterizations of genetic ablation and optogenetic inhibition experiments. a, **b**, Full distribution of nose poke preferences in individual animals in Fig. 2e (**a**) and Fig. 2g (**b**). Grey lines and dots indicate preferences of individual mice and colored line indicates the average across all animals. **c**, Representative trace showing robust silencing of Vgat^{+} neurons during light illumination. **d**, Firing rates before, during, and after light illumination. One-way repeated measures ANOVA with Bonferroni post-hoc correction ($^{***}P < 0.001$). **e**, **g**, Fraction of time spent on seven distinct social behaviors displayed by subject animals (**e**, GtACR-expressing animals, or **g**, control animals) towards juvenile animals. Two-way repeated measures ANOVA with Bonferroni post-hoc ($^{**}P < 0.01$, $^{***}P < 0.001$). **f**, **h**, Percentage of total time spent on all social behaviors displayed by subject animals (**f**, GtACR-expressing animals or **h**, control animals). $^{**}P = 0.0046$ (**f**), $P = 0.1766$ (**h**), paired t test (two-sided). (**a**, **b**) n = 8 control mice and 10 Caspase mice; (**c**, **d**) n = 10 trials from 3 cells (2 mice); (**e**-**h**), n = 6 control mice and 5 GtACR-expressing mice. (**d**-**h**) boxplots: center = median, box = quartiles, whisker = 10 – 90 percentile. For detailed statistics information, see Supplementary Table 1.

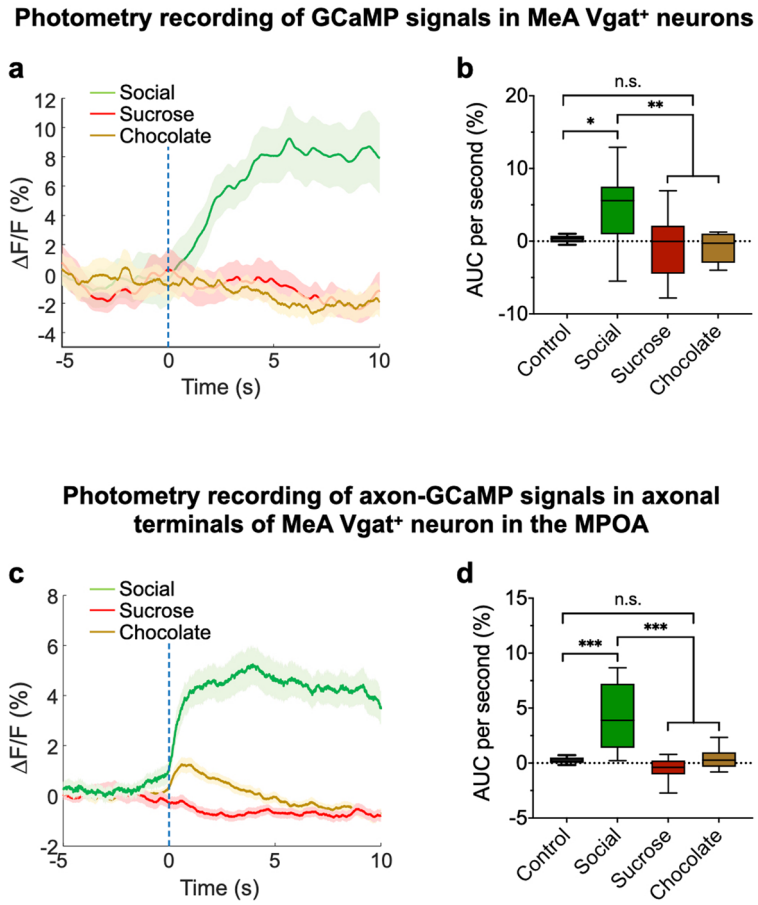

Extended Data Fig. 4 | Fiber photometry of calcium signals in response to social and nonsocial rewarding stimuli. MeApd Vgat$^+$ neurons and their projections to the MPOA are active in response to social stimuli, but not to nonsocial rewarding stimuli, such as sucrose and chocolate. **a**, **c**, Dynamics of Ca^{2+} signals ($\Delta F/F$) in MeApd Vgat$^+$ neurons (**a**) or in the axonal projections of MeApd Vgat$^+$ neurons to the MPOA (**c**) in response to social stimuli (juveniles) or during consumption of sucrose solution or chocolate. **b**, **d**, AUC per second under different conditions in **a** and **c**. Controls were done by measuring Ca^{2+} signals from EYFP-expressing MeApd Vgat$^+$ neurons or EYFP-expressing MeApd Vgat$^+$ neuron projections to the MPOA during exposure to social stimuli. One-way ANOVA with Bonferroni post-hoc correction ($^*P<0.05$, $^{**}P<0.01$, $^{***}P<0.001$). (**a**, **b**), n = 15 trials (social), 20 trials (sucrose), and 11 trials (chocolate) from 6 GCaMP7f-expressing mice; n = 22 trials (social) from 4 EYFP-expressing control mice. (**c**, **d**), n = 31 trials (social), 48 trials (sucrose), and 37 trials (chocolate) from 7 GCaMP6s-expressing mice; n = 17 trials (social) from 4 EYFP-expressing control mice. (**a**, **c**), mean ± SEM; (**b**, **d**), boxplots: center = median, box = quartiles, whisker = 10 – 90 percentile. For detailed statistics information, see Supplementary Table 1.

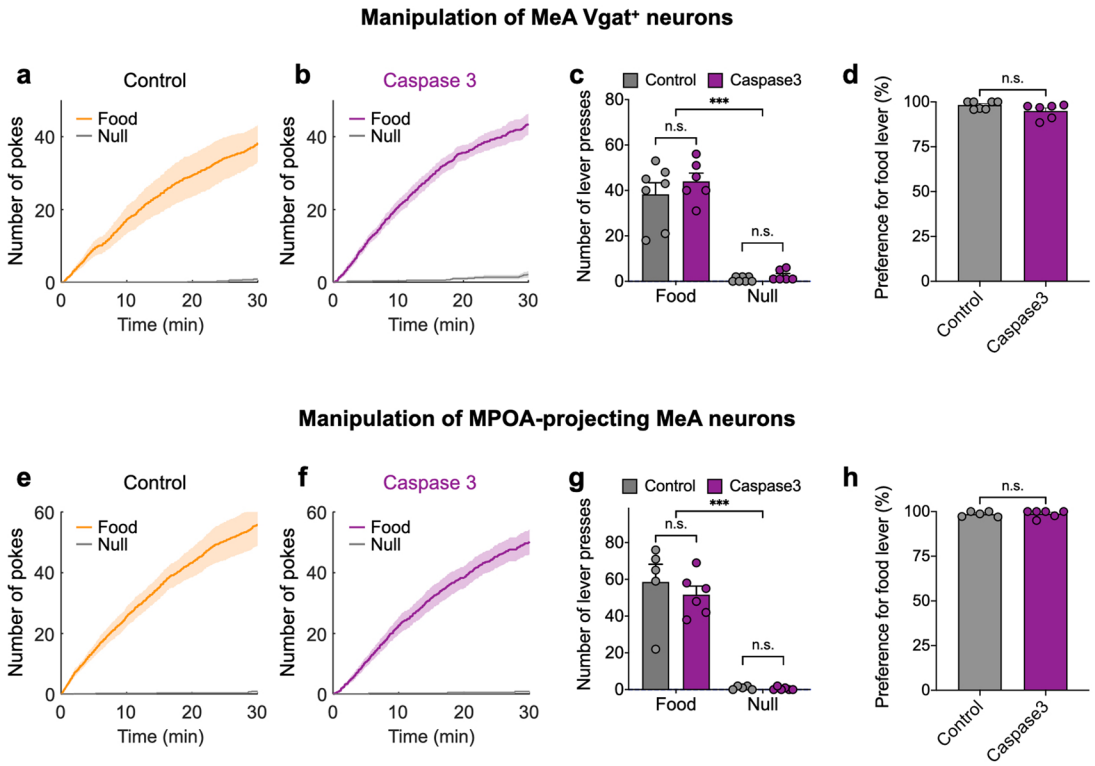

Extended Data Fig. 5 | The MeApd-to-MPOA circuit does not mediate food reward. a-d, Ablation of MeApd Vgat+ neurons does not affect food reward in an operant task. Animals are trained to lever press to obtain food pellets (see Methods). Control: animals expressing mCherry in MeApd Vgat+ neurons, Caspase 3: animals expressing Caspase 3 in MeApd Vgat+ neurons. **e-h**, Ablation of MPOA-projecting MeApd neurons does not affect food reward in an operant task. Control: animals expressing mCherry in MPOA-projecting MeApd neurons, Caspase 3: animals expressing Caspase 3 in MPOA-projecting MeApd neurons. **a**, **b**, **e**, **f**, cumulative distribution of lever presses in the operant task for food reward. **c**, **g**, number of lever presses. Two-way repeated measures ANOVA with Bonferroni post-hoc correction (***$P < 0.001$). **d**, **h**, preferences for the lever associated with food reward. Mann-Whitney test (two-sided). (**a**-**d**), n = 7 control mice and 6 Caspase mice; (**e**-**h**), n = 5 control mice and 6 Caspase mice; (**a**-**h**), mean ± SEM. For detailed statistics information, see Supplementary Table 1.

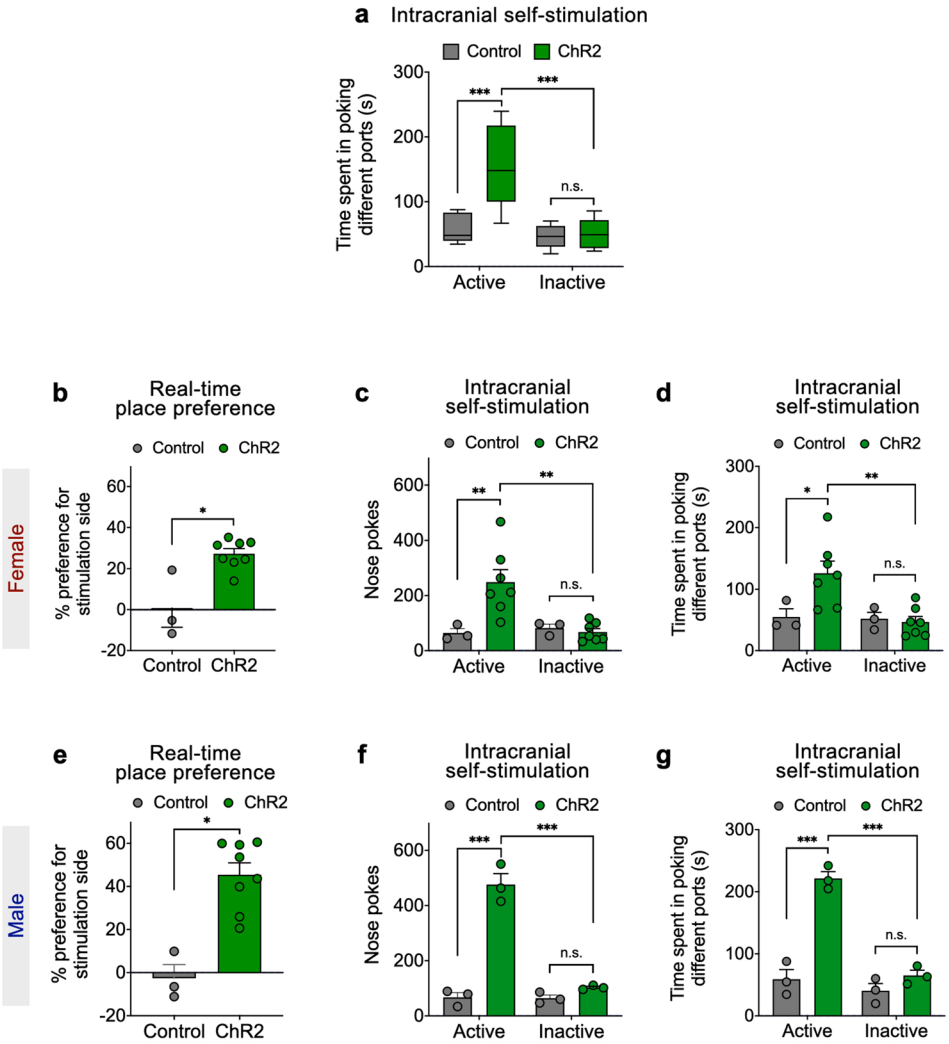

Extended Data Fig. 6 | Activation of MeApd Vgat⁺ neurons promotes reinforcement behavior in both males and females. a, Activation of MeApd Vgat⁺ neurons in the intracranial self-stimulation assay. ChR2-expressing animals spend greater time in the stimulation-coupled active port (total time spent in the port), whereas control animals do not. Two-way repeated measures ANOVA with Bonferroni post-hoc correction (***$P < 0.001$). **b**, **e**, In a real-time place preference assay, ChR2-expressing animals display a positive preference towards the stimulation-coupled chamber compared to the EYFP-expressing controls in both females (**b**) and males (**e**). *$P = 0.0242$ (**b**), *$P = 0.0121$ (**e**), Mann-Whitney test (two-sided). **c**, **f**, In an intracranial self-stimulation assay, ChR2-expressing female (**c**) and male (**f**) animals exhibit a greater number of pokes towards the active port compared to the inactive port, whereas control animals do not. Two-way repeated measures ANOVA with Bonferroni post-hoc correction (**p < 0.01, ***p < 0.001). **d**, **g**, ChR2-expressing female (**d**) and male (**g**) animals spend greater time in the active port (total time spent in the port), whereas control animals do not. Two-way repeated measures ANOVA with Bonferroni post-hoc correction (*$P < 0.05$, **$P < 0.01$, ***$P < 0.001$). (**a**), n = 6 control mice and 10 ChR2 mice; (**b**), n = 3 control mice and 8 ChR2 mice; (**c**-**d**), n = 3 control mice and 7 ChR2 mice; (**e**), n = 3 control mice and 8 ChR2 mice; (**f**-**g**), n = 3 control mice and 3 ChR2 mice. (**a**) boxplots: center = median, box = quartiles, whisker = 10 – 90 percentile; (**b**-**g**) mean ± SEM. For detailed statistics information, see Supplementary Table 1.

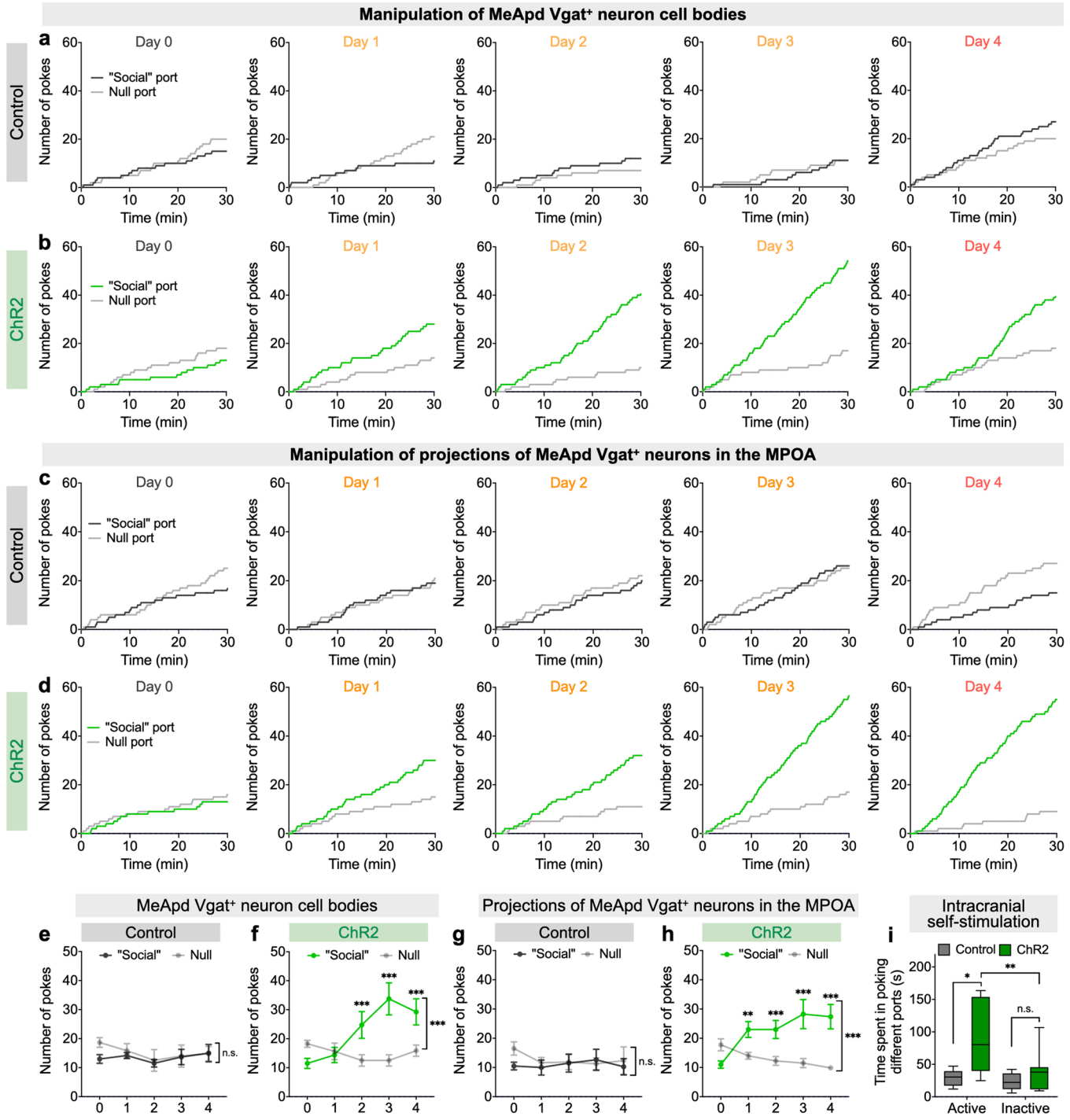

Extended Data Fig. 7 | Optogenetic activation of MeApd Vgat⁺ neurons or MeApd-to-MPOA projections drives reinforcement. a-d, Cumulative distribution of the numbers of nose pokes to the optogenetic 'social' port or the null port in a modified social operant task. Representative data from a control or ChR2 animal (**a**, **b**, MeApd cell bodies; **c**, **d**, MeApd-to-MPOA projections) on each day. **e-h**, Numbers of pokes to the optogenetic 'social' port or the null port on each day. For MeApd cell bodies, control (**e**) and ChR2-expressing (**f**) animals; for MeApd-to-MPOA projections, control (**g**) and ChR2-expressing (**h**) animals. Two-way repeated measures ANOVA with Bonferroni post-hoc correction (**$P < 0.01$, ***$P < 0.001$). **i**, Activation of MeApd-to-MPOA projections in ChR2-expressing animals spend greater time in the active port (total time spent in the port), whereas control animals do not. Two-way repeated measures ANOVA with Bonferroni post-hoc correction ((*$P < 0.05$, **$P < 0.01$). (**e**, **f**), n = 6 mice (control) and n = 8 mice (ChR2); (**g**, **h**), n = 8 mice (control) and n = 8 mice (ChR2); (**i**), n = 5 mice (control) and 7 mice (ChR2). (**e-h**), mean ± SEM; (**i**), boxplots: center = median, box = quartiles, whisker = 10 – 90 percentile. For detailed statistics information, see Supplementary Table 1.

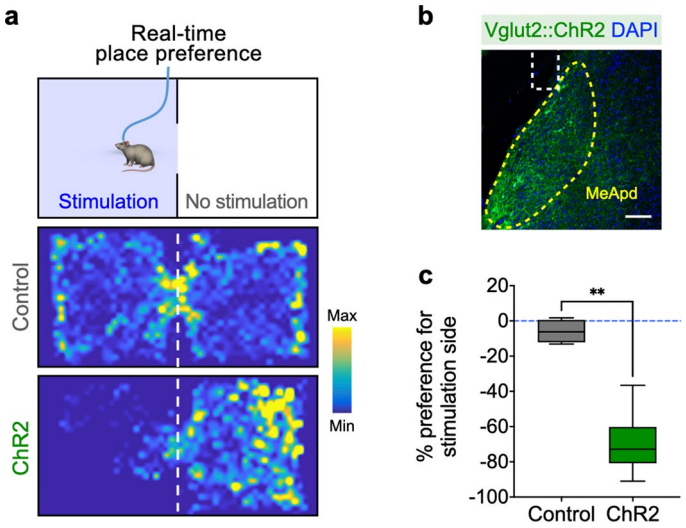

Extended Data Fig. 8 | Optogenetic activation of MeApd Vglut2$^+$ neurons promotes place aversion. a, Schematic showing the real-time place preference assay (RTPP). Light blue area (top) indicates the chamber paired with light stimulation when the mouse enters. Representative heatmaps showing locomotion trajectories for controls (middle) and ChR2-experessing (bottom) Vglut2-Cre mice in the RTPP test. **b**, Example image of viral expression in the MeApd of Vglut2-Cre animals. Scale bar = 200 µm. **c**, ChR2-expressing Vglut2-Cre animals display a negative preference towards the stimulation-couple chamber compared to EYFP-expressing controls. n = 4 mice (control) and 6 mice (ChR2). $^{**}P = 0.0095$, Mann-Whitney test (two-sided). Boxplots: center = median, box = quartiles, whisker = 10 – 90 percentile. For detailed statistics information, see Supplementary Table 1.

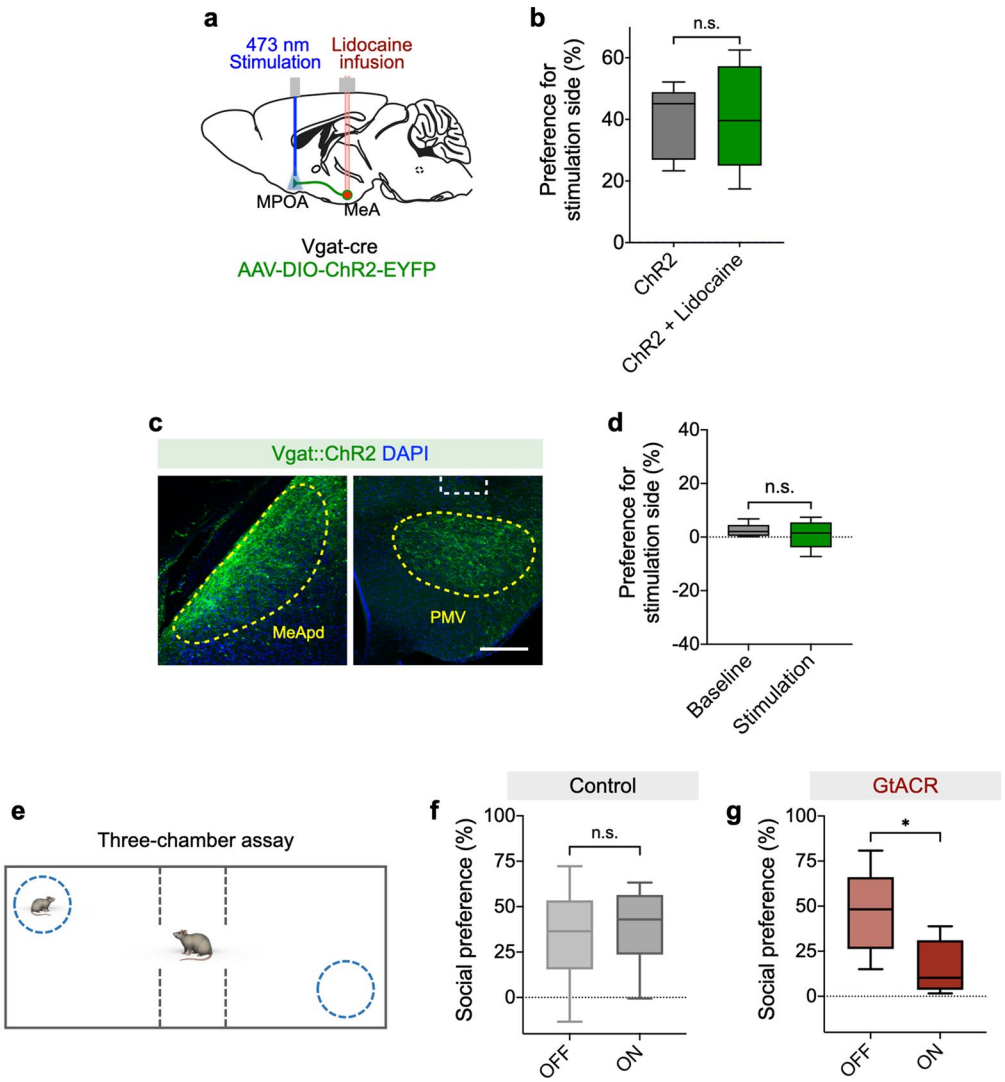

Extended Data Fig. 9 | Behavioral functions of MeA-to-MPOA and MeA-to-PMV pathways. a, Schematic showing optogenetic stimulation of MeApd axon terminals in the MPOA and lidocaine infusion in the MeApd cell bodies. **b**, Local infusion of lidocaine in the MeApd does not affect the behavioral effect of stimulating the MeApd-to-MPOA projection. $P = 0.7612$, paired t test (two-sided). **c-d**, Activating the MeApd-to-PMV projection does not promote positive reinforcement. **c**, Example images showing expression of ChR2 in the MeApd Vgat$^+$ neurons (left) and fiber placement above their axon terminals in the PMV (right). Scale bar = 200 μm. **d**, Optogenetic stimulation of MeApd Vgat$^+$ neuron terminals in the PMV does not produce positive place preference in a real-time place preference assay. $P = 0.5103$, paired t test (two-sided). **e-g**. Suppressing MeApd Vgat$^+$ neuron activity reduces social preference in a three-chamber assay**. e**, Schematic showing the three-chamber assay. **f-g**, Optogenetic inhibition of MPOA-projecting MeA neurons in GtACR-expressing mice (**g**), but not in control mice (**f**), reduces social preference in a three-chamber social preference assay. $P = 0.7183$ (**f**), $^*P = 0.0471$ (**g**), paired t test (two-sided). (**b**), n = 5 ChR2-expressing mice; (**c**, **d**), n = 6 ChR2-expressing mice; (**f-g**), n = 6 control mice and 5 GtACR-expressing mice. Boxplots: center = median, box = quartiles, whisker = 10 – 90 percentile. For detailed statistics information, see Supplementary Table 1.

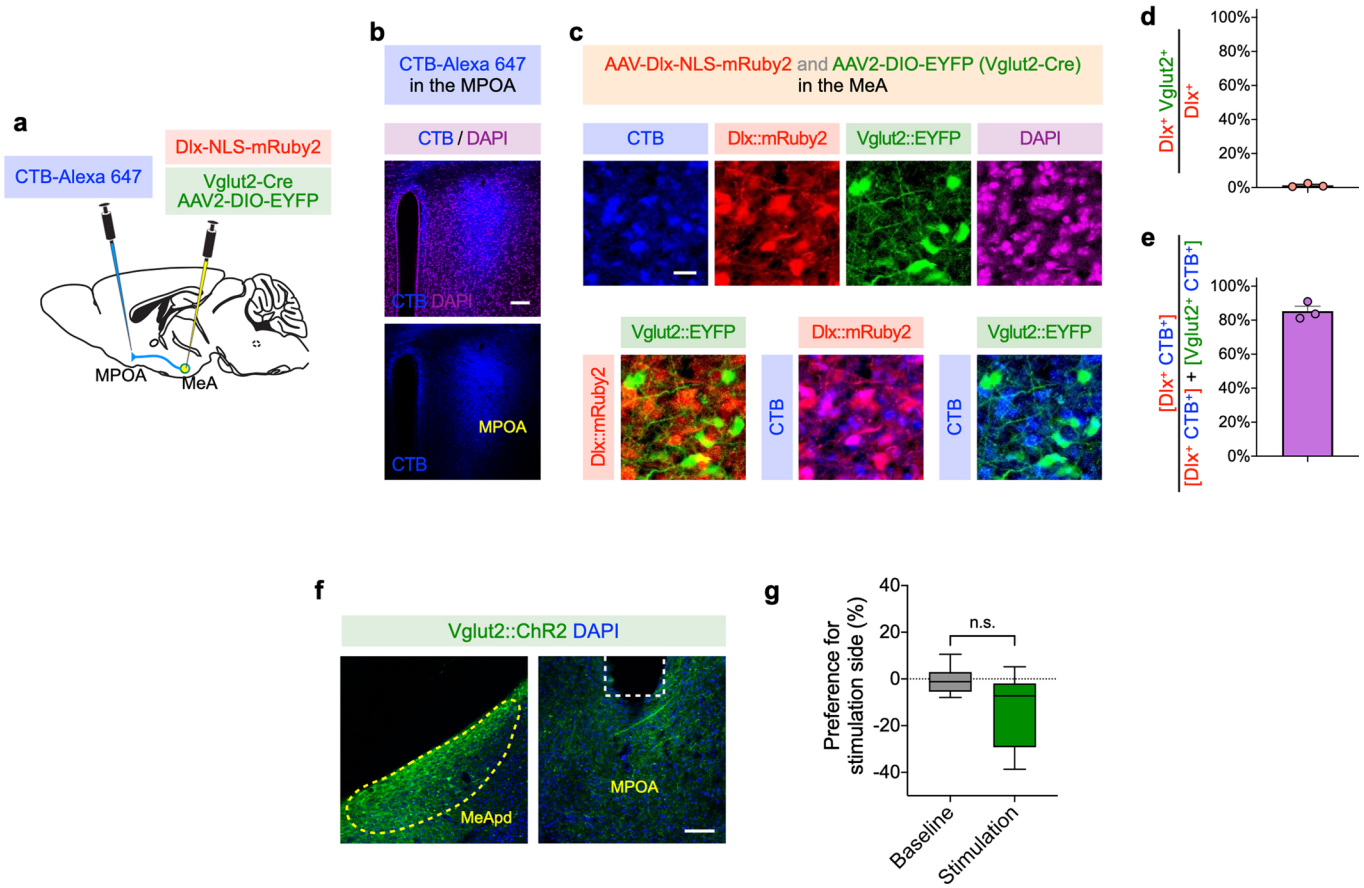

Extended Data Fig. 10 | Characterization of MeApd neurons projecting to the MPOA. a, Schematic showing injections of CTB-Alexa 647 into the MPOA and AAV-Dlx-NLS-Ruby2 and AAV-DIO-EYFP into the MeApd of Vglut2-Cre animals. **b**, Representative images showing labeling of CTB-Alexa 647 in the MPOA. Scale bar = 100 μm. **c**, Representative images showing retrogradely labeled CTB-Alexa 647 with the expression of AAV-Dlx-NLS-Ruby2 and AAV-DIO-EYFP in the MeApd of Vglut2-Cre animals. Scale bar = 20 μm. **d**, The fraction of overlap between Dlx$^+$ and Vglut2$^+$ neurons among all Dlx$^+$ neurons. We confirm that the expression of Dlx and Vglut2 promotors shows little overlap in the MeApd. **e**, Fraction of MPOA-projecting MeApd neurons that are GABAergic. The majority of the MeApd neurons that project to the MPOA are GABAergic. **f**, Representative images showing expression of ChR2 in the MeApd Vglut2$^+$ neurons (left) and fiber placement above their axon terminals in the MPOA (right) of Vglut2-Cre animals. Scale bar = 100 μm. **g**, Activating the MeApd Vglut2$^+$ projections to the MPOA does not drive place preference. $P = 0.1958$, Paired t test (two-sided). (**b**-**e**), n = 3 mice; (**f**, **g**), n = 6 ChR2 mice. (**d**, **e**), mean ± SEM; (**g**), Boxplots: center = median, box = quartiles, whisker = 10 – 90 percentile. For detailed statistics information, see Supplementary Table 1.

nature research

Corresponding author(s): Weizhe Hong

Last updated by author(s): 2/20/2021

Reporting Summary

Nature Research wishes to improve the reproducibility of the work that we publish. This form provides structure for consistency and transparency in reporting. For further information on Nature Research policies, see our Editorial Policies and the Editorial Policy Checklist.

Statistics

For all statistical analyses, confirm that the following items are present in the figure legend, table legend, main text, or Methods section.

n/a	Confirmed	
☐	☒	The exact sample size (*n*) for each experimental group/condition, given as a discrete number and unit of measurement
☐	☒	A statement on whether measurements were taken from distinct samples or whether the same sample was measured repeatedly
☐	☒	The statistical test(s) used AND whether they are one- or two-sided *Only common tests should be described solely by name; describe more complex techniques in the Methods section.*
☐	☒	A description of all covariates tested
☐	☒	A description of any assumptions or corrections, such as tests of normality and adjustment for multiple comparisons
☐	☒	A full description of the statistical parameters including central tendency (e.g. means) or other basic estimates (e.g. regression coefficient) AND variation (e.g. standard deviation) or associated estimates of uncertainty (e.g. confidence intervals)
☐	☒	For null hypothesis testing, the test statistic (e.g. *F*, *t*, *r*) with confidence intervals, effect sizes, degrees of freedom and *P* value noted *Give P values as exact values whenever suitable.*
☒	☐	For Bayesian analysis, information on the choice of priors and Markov chain Monte Carlo settings
☒	☐	For hierarchical and complex designs, identification of the appropriate level for tests and full reporting of outcomes
☒	☐	Estimates of effect sizes (e.g. Cohen's *d*, Pearson's *r*), indicating how they were calculated

Our web collection on statistics for biologists contains articles on many of the points above.

Software and code

Policy information about availability of computer code

Data collection	Behavior data was acquired through an Arduino microcontroller board or a video camera (FLIR). Photometry data was acquired using CED Micro 1401 and Spike2 version 8.03.
Data analysis	Data were processed and analyzed in MATLAB 2018b (MathWorks). MATLAB code that is used to analyze behavior is available at https://pdollar.github.io/toolbox/. Figures were plotted using Prism GraphPad 9 (GraphPad Software) or MATLAB 2018b (MathWorks).

For manuscripts utilizing custom algorithms or software that are central to the research but not yet described in published literature, software must be made available to editors and reviewers. We strongly encourage code deposition in a community repository (e.g. GitHub). See the Nature Research guidelines for submitting code & software for further information.

Data

Policy information about availability of data

All manuscripts must include a data availability statement. This statement should provide the following information, where applicable:

- Accession codes, unique identifiers, or web links for publicly available datasets
- A list of figures that have associated raw data
- A description of any restrictions on data availability

The data that support the findings of this study are available from the corresponding author upon reasonable request.

Field-specific reporting

Please select the one below that is the best fit for your research. If you are not sure, read the appropriate sections before making your selection.

☒ Life sciences ☐ Behavioural & social sciences ☐ Ecological, evolutionary & environmental sciences

For a reference copy of the document with all sections, see nature.com/documents/nr-reporting-summary-flat.pdf

Life sciences study design

All studies must disclose on these points even when the disclosure is negative.

Sample size	No statistical methods were used to pre-determine sample sizes, but our sample sizes were selected based on previous experience from related research and literature. Sample size for each experiment is described in the Supplementary Table 1.
Data exclusions	Animals that exhibited no or little motivation to engage in nose-pokes on the first two days of training (defined as less than 10 total pokes of social and null ports on each day) were excluded from training and data collection. One EYFP-expressing animal in the photometry experiment was excluded based on this criterion. Animals that had low body weight (males <20 g and females <16 g) were excluded from surgeries and experiments.
Replication	Experiments were independently performed in multiple different animals. The number of different animals used is described in the Supplemental Table 1. Our findings are reliably reproduced in at least two independent cohorts of animals.
Randomization	Animals were randomly assigned to control and manipulation groups.
Blinding	Data collection and analysis were not performed blind to the conditions of experiments.

Reporting for specific materials, systems and methods

We require information from authors about some types of materials, experimental systems and methods used in many studies. Here, indicate whether each material, system or method listed is relevant to your study. If you are not sure if a list item applies to your research, read the appropriate section before selecting a response.

Materials & experimental systems

n/a	Involved in the study
☐	☒ Antibodies
☒	☐ Eukaryotic cell lines
☒	☐ Palaeontology and archaeology
☐	☒ Animals and other organisms
☒	☐ Human research participants
☒	☐ Clinical data
☒	☐ Dual use research of concern

Methods

n/a	Involved in the study
☒	☐ ChIP-seq
☒	☐ Flow cytometry
☒	☐ MRI-based neuroimaging

Antibodies

Antibodies used	Chicken Anti-GFP antibody (Aves Labs #1020); donkey anti-chicken Alexa 488 antibody (Jackson ImmunoResearch #703-545-155)
Validation	Chicken Anti-GFP antibody was validated using tissues with and without dLight expression. Quality control information and relevant citations are available at manufacturer's website (https://www.aveslabs.com/products/green-fluorescent-protein-gfp-antibody)

Animals and other organisms

Policy information about studies involving animals; ARRIVE guidelines recommended for reporting animal research

Laboratory animals	C57BL/6J males and females (8-12 weeks old) were purchased from Jackson Laboratories and used for behavioral experiments. Slc32a1-ires-Cre (Vgat-Cre) and Slc17a6-ires-Cre (Vglut2-Cre) mice were purchased from Jackson Laboratories (stock number 028862 and 028863) and were crossed to C57BL/6J mice to produce heterozygous animals (8-16 weeks old, both males and females) for stereotaxic surgery and behavioral experiments.
Wild animals	No wild animals were used in the study
Field-collected samples	No field collected samples were used in the study.

Ethics oversight	All experiments were carried out in accordance with the NIH guidelines and approved by the UCLA institutional animal care and use committee (IACUC).

Note that full information on the approval of the study protocol must also be provided in the manuscript.